electronics

MDPI

Review

Plasma Treatment Technologies for GaN Electronics

Botong Li [1], Imteaz Rahaman [1], Hunter D. Ellis [1], Houqiang Fu [2], Yuji Zhao [3], Yong Cai [4,5], Baoshun Zhang [4,5] and Kai Fu [1,*]

[1] Electrical and Computer Engineering, The University of Utah, Salt Lake City, UT 84112, USA; u1540316@utah.edu (B.L.); u1351894@utah.edu (I.R.); u0973796@utah.edu (H.D.E.)
[2] School of Electrical, Computer and Energy Engineering, Arizona State University, Tempe, AZ 85281, USA; houqiang@asu.edu
[3] Department of Electrical and Computer Engineering, Rice University, Houston, TX 77005, USA; yuji.zhao@rice.edu
[4] The Nanofabrication Facility, Suzhou Institute of Nano-Tech and Nano-Bionics, Chinese Academy of Sciences, Suzhou 215123, China; ycai2008@sinano.ac.cn (Y.C.); bszhang2006@sinano.ac.cn (B.Z.)
[5] The School of Nano-Tech and Nano-Bionics, University of Science and Technology of China, Hefei 230026, China
* Correspondence: kai.fu@utah.edu

Abstract: Nowadays, the third-generation semiconductor led by GaN has brought great changes to the semiconductor industry. Utilizing its characteristics of a wide bandgap, high breakdown Electric field, and high electron mobility, GaN material is widely applied in areas such as 5G communication and electric vehicles to improve energy conservation and reduce emissions. However, with the progress in the development of GaN electronics, surface and interface defects have become a main problem that limits the further promotion of their performance and stability, increasing leakage current and causing degradation in breakdown voltage. Thus, to reduce the damage, Plasma treatment technologies are introduced in the fabrication process of GaN electronics. Up to now, designs like the high-resistivity p-GaN cap Layer, passivating termination, and surface recovery process have been established via Plasma treatment, reaching the goals of normally-off transistors, diodes with high breakdown voltage and high-reliability GaN electronics, etc. In this article, hydrogen, fluorine, oxygen, and nitrogen Plasma treatment technologies will be discussed, and their application in GaN electronics will be reviewed and compared.

Keywords: GaN; Plasma treatment; power electronics; sensor

check for updates

Citation: Li, B.; Rahaman, I.; Ellis, H.D.; Fu, H.; Zhao, Y.; Cai, Y.; Zhang, B.; Fu, K. Plasma Treatment Technologies for GaN Electronics. *Electronics* **2024**, *13*, 4343. https://doi.org/10.3390/electronics13224343

Academic Editors: Byung-Gyu Kim, Costas Psychalinos, Victor Erokhin and Zhengran He

Received: 12 September 2024
Revised: 25 October 2024
Accepted: 30 October 2024
Published: 6 November 2024

Copyright: © 2024 by the authors. Licensee MDPI, Basel, Switzerland. This article is an open access article distributed under the terms and conditions of the Creative Commons Attribution (CC BY) license (https://creativecommons.org/licenses/by/4.0/).

1. Introduction

The development of modern society is closely related to the application of various electronic devices [1]. Since the first transistor was produced by Bell LABS in 1947, power electronic devices, dominated by silicon-based devices, have been widely used in telecommunication [2–4], power transmission and distribution [5–7], consumer electronics [8–10], electric vehicles [11–13], industrial motor drives [14–16], data centers [17–19], smart grids [20–22], etc., which have strongly promoted the development and progress of electronic technology and even the entirety of human society [23–25]. At present, with the development of technology, the modern power electronics field has experienced an increasingly strong demand for high-voltage and high-frequency applications [26–29], which is consistent with the prediction made by Moore's Law about the constant advancement of miniaturization, high integration [30,31], high power Density, and high performance of the electronic devices [26,32,33]. Due to this demand, the performance of silicon-based devices has gradually approached its limit due to their narrow bandgap and low breakdown Electric field, facing difficulties in integration and efficiency under high power circumstances. Therefore, the search for semiconductor materials with better properties to meet the challenges brought by industrial upgrading has become a new research focus in the field of electronics [34–36].

To solve this problem, third-generation semiconductors with silicon carbide (SiC) and gallium nitride (GaN) as the main materials have been extensively explored [37–39]. The research on second-generation semiconductors (GaAs and InP) has already revealed that the larger bandgap property can provide high stability and energy transmission efficiency [40–44]. It is believed that third-generation semiconductors (GaN and SiC) with a larger bandgap, higher breakdown Electric field, and higher saturation velocity can provide great integration Density and power performance for devices compared to traditional silicon semiconductors [45–49]. Table 1 lists the basic material characteristics of different semiconductor materials [33,50–52]. From this comparison, GaN stands out with the largest bandgap and the highest breakdown Electric field. It also has excellent electron mobility and good thermal conductivity. For intuitively representing the power electronic performance of semiconductors, Baliga's figure of merit (BFOM) is also introduced, here, from the relationship between breakdown voltage and the on-resistances as follows:

$$R_{on} = \frac{4BV^2}{\varepsilon_S \mu_n E_C^3} \tag{1}$$

$$BFOM = \varepsilon_S \mu_n E_C^3 \tag{2}$$

where ε_s, μ_n, and E_C are the relative dielectric constant, electron mobility, and breakdown Electric field, respectively [27,53,54]. Also, as seen in Table 1, the BFOM of GaN only ranks second to the diamond material, proving its superiority in power applications. On this basis, the further development of large-scale epitaxy of GaN on low-cost silicon Substrate provides the cost guarantee for GaN-based devices [55,56]. With all of these properties, GaN has already become one of the most promising candidates for the core material in future electronics.

Table 1. A comparison of the physical properties of GaN, Si, GaAs, SiC, and InP [52].

Property	GaN	Si	GaAs	SiC	InP	Diamond
Dielectric constant [ε_s]	9.5	11.4	13.1	9.7	12.5	5.5
Bandgap [E_g (eV)]	3.4	1.1	1.4	2.9	1.35	5.5
Electron mobility [μ (cm^2/Vs)]	2000	1300	5000	260	5400	2000
Breakdown Electric field [E_C (MV/cm)]	3.3	0.3	0.4	2.5	0.5	10
Thermal conductivity [χ (W/cm·K)]	1.3	1.5	0.46	4.9	0.7	20
Saturation drift velocity [V_{sat} ($\times 10^7$ cm/s)]	2.2	1.0	1.0	2.0	1.0	2.7

Since Khan et al. first fabricated the two-dimensional electron gas (2DEG) at the AlGaN/GaN interface in 1992, GaN-based high electron mobility transistors (HEMTs) have remained a focal point of research in wide bandgap semiconductor devices [57–59]. As seen in Figure 1, the energy band structure of the AlGaN/GaN interface shares the same mechanism of AlGaAs/GaAs heterojunction, but its high 2DEG concentration over 1×10^{13} cm^{-2}, caused by the polarization effect, makes it more advantageous in the application of a microwave high-temperature and high-power device [60]. Over the past two decades, significant achievements have been made in GaN HEMTs. Novel structures, such as the recessed gate [61–63], the p-GaN gate [64,65], the passivation Layer, and field plates, were invented, promoting the application and commercialization of GaN-based devices [66–69]. However, during the fabrication and measurement of GaN HEMTs, researchers have found that the properties of the surface and interface seriously affected the device's performance [70]. Fabricating processes, like etching, can easily introduce interface states and surface dangling bonds into the devices, causing the effect of premature breakdown and threshold voltage offset, etc. [71,72]. Therefore, it is reasonable to introduce Plasma treatment techniques to alleviate the damage and preciously modulate the device's performance [73,74].

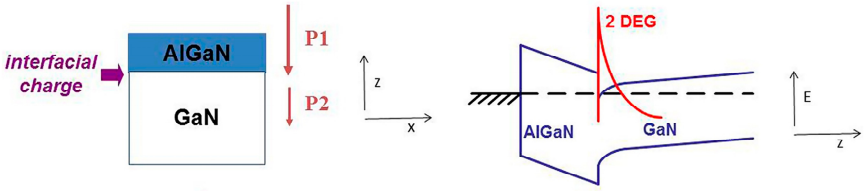

Figure 1. A schematic structure and band diagram of an AlGaN/GaN FET heterojunction, showing the formation of 2D electron gas [60]. Copyright 2019, Elsevier.

Plasma processes for GaN were largely driven by advancements in GaN optoelectronics during the 1990s, particularly in its early development stages. Plasma processes were employed in GaN optoelectronic devices for various applications, such as etching (using Cl_2 and CH_4 Plasma) [75–80], surface cleaning [81–83], and damage repair [84–86]. During these applications, researchers studied the Plasma-induced damage, which manifested in several ways, including ion-induced lattice defects, unintentional dopant passivation, the creation of non-stoichiometric surfaces, and the deposition of polymeric films [87]. Through inductively coupled Plasma (ICP) devices, the power and Density of Plasma can be controlled to change the material characteristics, such as the resistivity and carrier Density. In recent years, Plasma treatment has been widely used in electronics fabrication. Progress like high-performance enhancement mode, high breakdown voltage, and high thermal stability in GaN HEMTs has been achieved [88,89], proving the effectiveness and good application prospects of Plasma treatment techniques.

In this paper, the origin, mechanism, and recent progress of Plasma treatment technologies for GaN electronics will be reviewed and discussed. This review will begin by discussing hydrogen Plasma and fluorine Plasma treatments for GaN electronics, focusing on their specific processes and innovative device structure designs. Oxygen and nitrogen Plasma treatments and a comparison between different processing techniques will also be shown as a supplement to this review.

2. Hydrogen Plasma Treatment for GaN HEMTs

2.1. The Mechanism of H Plasma Treatment

The passivation effect of the hydrogen atom in p-type GaN was first studied by Nakamura et al. in 1992 [90]. Two different annealing atmospheres were adopted after the GaN epitaxy. The high resistivity of 1×10^6 Ω·cm was reached in the p-GaN films under the NH_3 atmosphere, while the film under the N_2 atmosphere showed almost no change in resistivity, revealing the passivation effect of hydrogen on holes in p-GaN. Such a phenomenon was further explained by Polyakov et al. in 2003 [91]. Their micro cathodoluminescence measurement on the p-GaN sample before and after H Plasma exposure at 250 °C showed that the donor–acceptor pairs (DAP) intensity was significantly decreased after the treatment, indicating a great decrease in hole concentration in the near-surface region. The temperature dependence of the DC current was also measured in their study. Subsequently, by extracting the conductivity decreasing value, it was found that the conductivity decrease was lower than a factor of 10 from the hole concentration decrease observed from C-V profiling. This indicates that the increase in hole mobility after Plasma exposure is more likely due to the passivation of Mg acceptors rather than the formation of compensating centers. In 2012, Chen et al. also studied the recovering effect of H Plasma treatment on etched GaN surfaces [92]. The obvious increase in the XPS intensity of Ga-H bonds demonstrated the passivation of H Plasma on nitrogen vacancies.

2.2. H Plasma Treatment for GaN HEMT

2.2.1. The Application of H Plasma Treatment

According to the above theory, H Plasma treatment was introduced in the fabrication of enhancement-mode (E-mode) GaN HEMTs by Hao et al. in 2016 [73]. In 2000, Hu et al. established the first p-GaN gate normally-off HEMT [93]. By growing a thin Layer of

p-GaN on the AlGaN/GaN heterostructure before the gate deposition, the gate control ability was enhanced at the formation of the p-n junction depletion region. For recovering the 2DEG in the p-GaN cap HEMT, the etching method with the source of Cl_2/BCl_3 [94], $Cl_2/BCl_3/CHF_3$, and $Cl_2/O_2/N_2$ was first applied [95]. The enhancement mode was achieved, but the current instability had become a severe problem under pulsed conditions. Thus, in the study by Hao et al., 5 min of hydrogen Plasma treatment was applied on the p-GaN Layer using gate metal as the hard mask to selectively decrease the hole Density [73]. Hence, the conduction band was pulled below the Fermi level, reestablishing the 2DEG in the Channel. The as-grown and Cl_2/BCl_3 etched devices were also fabricated as a comparison for the Plasma-treated one, and the schematic diagram can be seen in Figure 2a–c, named devices A, B, and C, respectively. Figure 2d–g show the comparison of transfer characteristics among different devices. As seen in the comparison between devices A and C, the threshold voltage (Vth), saturation current, and transconductance were increased to 1.75 V, 188 mA/mm, and 73.1 mS/mm, respectively, and meanwhile, the gate leakage current was suppressed. The increment of the saturation current was also observed in the comparison between devices B and C, which partially proved the superiority of H Plasma technology.

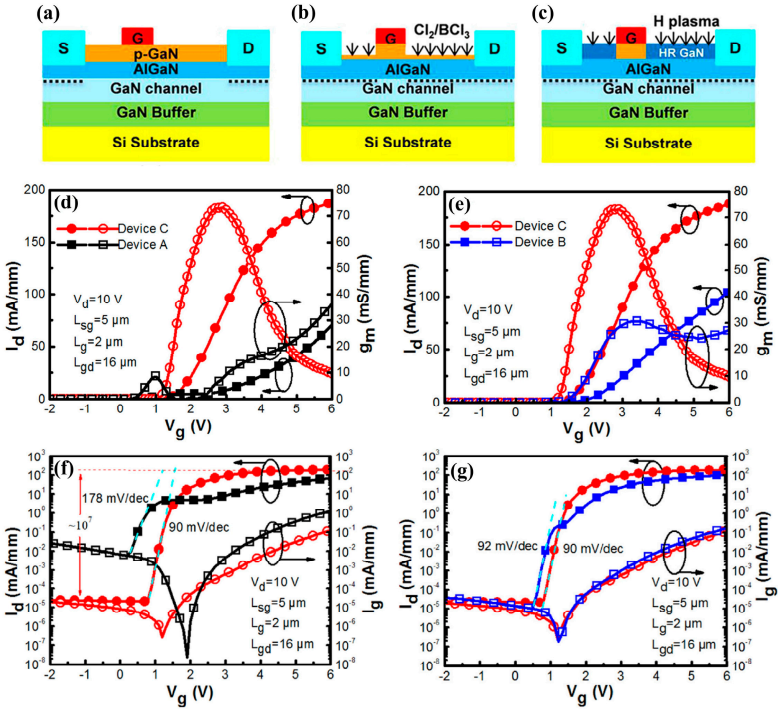

Figure 2. Cross-sectional comparison of devices processed using different methods: (**a**) Device A: as-grown, (**b**) Device B: etched with Cl_2/BCl_3, and (**c**) Device C: treated with H Plasma. I_d–V_g and transconductance characteristics are shown for (**d**) Device A vs. Device C and (**e**) Device B vs. Device C. I_d–V_g characteristics in logarithmic scale are presented for (**f**) Device A vs. Device C and (**g**) Device B vs. Device C [73]. Copyright 2016, AIP publishing.

The comparison between H Plasma treatment and the traditional etching process was further studied by Li et al. [96]. In this study, the etched and the H Plasma-treated HEMT were monolithically fabricated on the 4-in wafer, as shown in Figure 3a. The OFF-state stress test result for both V_{TH} shifts is presented in Figure 3c,d. While the stress had little effect on the value of V_{TH} between the H Plasma-treated and etched devices, the linear scale of the transfer curves showed a clear current degradation for the etched device. Further tests of the Vth shift under both soft-switching and hard-switching conditions are presented in Figure 3e,f. The H-treated device, here, exhibited enhanced stability in V_{TH} compared to the etched one, partially suggesting the efficacy of the hydrogen Plasma

treatment. Figure 3g,h exhibit another measurement of the corresponding changes in drain current (I_D), Extracted under soft- and hard-switching. A modest 5% reduction in the current of H-treated devices indicated better resilience, while the etched device suffered from a substantial 48% reduction. Since the hot electron effect caused by the interface traps was the main reason for the performance degradation under hard-switching conditions, it can be concluded that the improved surface states and device stability were reached via H Plasma treatment [97–99].

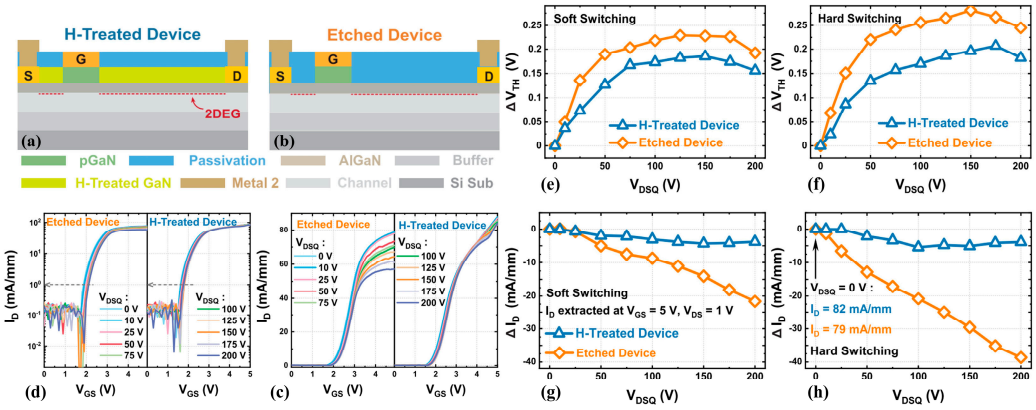

Figure 3. Schematic of (**a**) H-treated devices and (**b**) etched devices. Demonstration of measured (**c**) log and (**d**) linear transfer curves under OFF-state drain stress. V_{TH} shift under (**e**) soft-switching and (**f**) hard-switching conditions. I_D changes under (**g**) soft-switching and (**h**) hard-switching conditions [96]. Copyright 2024, IEEE.

2.2.2. The Optimization of H Plasma Treatment

After the realization of H-treated normally-off GaN, Hao et al. further studied the H-treatment parameters that affect the HEMTs' performances [89]. The transfer characteristics of devices fabricated with different H Plasma RF powers are shown in Figure 4a,b, with an ICP power of 300 W and a processing time of 5 min. The decrease in maximum drain current as the RF power increased came from the rise of treatment depth, while the higher reverse current indicated the damage caused by high-power Plasma treatment. The repairing of these damages was then realized via rapid thermal annealing (RTA). As seen in Figure 4c,d, the device at the Annealing Temperature of 350 °C shows the lowest reverse drain current and the highest maximum drain current, proving that an appropriate Annealing Temperature to recover the Plasma damage was found. Afterward, by applying the RTA process on all devices treated by different RF powers, a similar maximum drain current, but a different reverse current, was observed. Such variation in the trend demonstrated that the high RF power is not necessary for a high drain current after the RTA process, and the standard H Plasma treatment with RTA repairing was established for the E-mode GaN HEMTs fabrication [100].

In fact, the RTA is not the only way to solve the above-mentioned Plasma damage. In 2021, Sun et al. introduced the surface-etching method in the H Plasma treatment process [101]. The ICP etching device was adopted to remove 5 nm of p-GaN at a rate of 1.6 nm/min, as seen in Figure 5a. The suppression of gate leakage current proved that the surface-etching process is an effective method for Plasma damage repair. In addition to repair after treatment, reducing the damage of Plasma treatment is also a common method [102,103]. For example, Huang et al. optimized the H Plasma treatment process by depositing a thin SiN_x film before H Plasma implantation in 2022 [104]. A schematic diagram is depicted in Figure 5b. DC current measurement showed that a significant decrease in leakage current and on-resistance was achieved after the optimization. The similar effect of the Al_2O_3 passivation Layer was also proved by them in the same year [105]. Recently, Han et al. further developed the Si_3N_4/Al_2O_3 stacked passivation structure, and the improved suppression of gate reverse leakage current was realized [106].

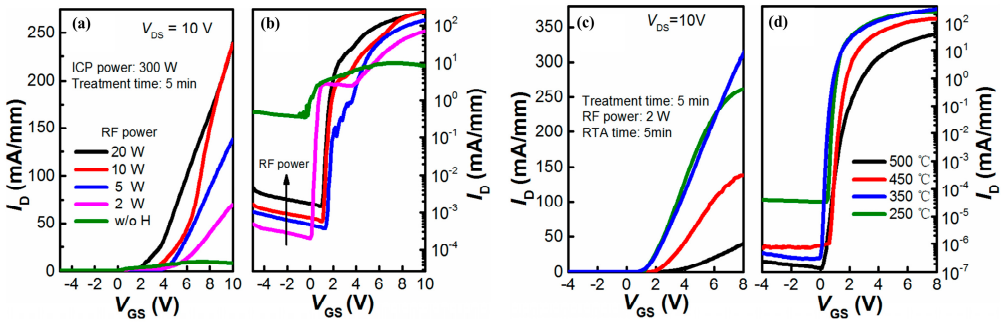

Figure 4. The transfer characteristics of E-mode GaN HEMTs with varying hydrogen Plasma treatment RF powers are shown in (**a**) linear scale and (**b**) logarithmic scale. The transfer characteristics of the device treated at 2W RF power followed by RTA at different temperatures are presented in (**c**) linear scale and (**d**) logarithmic scale [89]. Copyright 2018, IEEE.

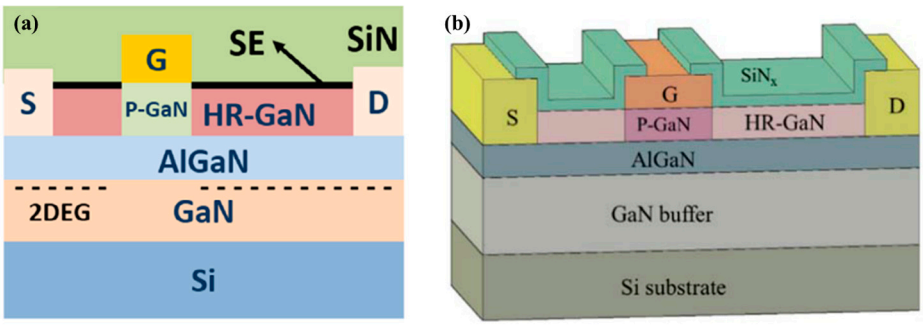

Figure 5. Schematic cross sections of (**a**) self-etched and (**b**) SiN_x passivated H-treated GaN HEMTs [105]. Reproduced with permission from Acta Physica Sinica.

2.2.3. Recent Progress of H Plasma-Treated GaN Devices

In recent years, various studies on the design and fabrication of novel H-treated GaN HEMTs have been established. In 2018, Hao et al. fabricated a 49.7 mm gate width normally-off GaN HEMT [107]. According to Figure 6a,b, the high-resistivity cap Layer (HRCL) was demonstrated using hydrogen Plasma treatment. A high threshold voltage of 2.5 V, a maximum drain current of 10 A, a breakdown voltage of 567 V, and a low gate leakage current of 1.3×10^{-7} A/mm were achieved at V_{GS} = 8 V. In the next year, the monolithic integration of enhancement-mode and depletion-mode GaN HEMTs was also realized via H Plasma treatment by Hao et al., as seen in Figure 6c [108]. This direct-coupled field-effect transistor logic (DCFL) system demonstrated a wide output logic swing of 4.78 V, an ultra-low threshold hysteresis of 13 mV, stable performance up to 300 °C, and a propagation delay of 0.8 ns/stage at V_{DD} = 5 V. The normally-off etching-free p-GaN stripe array gate AlGaN/GaN HEMTs (PSAG-HEMTs) designed by Wei et al. are also worth mentioning [109]. The PSAG shown in Figure 6d was fabricated through hydrogen Plasma treatment produced by the ICP device, using electron beam lithography as the pattern mask. According to a report by Wei et al., the V_{TH} can be continuously modulated by tuning the widths of p-GaN stripes, and the low $R_{ON,sp}$ of 2.73 mΩ·cm^2 and a high BV of 1449 could be reached at the optimized p-GaN extension length of 4 µm.

Except for the n-Channel devices, the GaN/AlN heterojunction p-Channel GaN HEMT is also a critical component in GaN power IC technology [110–112]. Due to the thick p-GaN Layer in the gate region, the common realization of the E-mode is the etched recessed gate. However, such devices usually suffer from high off-state leakages and reliability concerns caused by ion bombardment damage [113–115]. Thus, utilizing the damage-less characteristic of H Plasma treatment, the E-mode, Gate-Recess-Free, GaN-Based p-Channel HEMT was established [116]. The energy band diagram under the gate region illustrated in Figure 7 shows that, under the negative gate bias, the Fermi level of the Channel shifts upward as hole concentration increases, facilitating the transition to enhancement-mode

operation. The negative *V*th of −0.6 V, a peak transconductance of 0.22 mS/mm, and a high on/off ratio of 5×10^7 was also Extracted from the transfer characteristic. Additionally, the slight gate trench formed by slow etching can also help the performance improvement of this design [117]. According to the schematic and transfer curve in Figure 8a,b, even the negative *V*th and on/off ratio of 1×10^7 was achieved when combining a 30 nm deep gate trench with an H passivated p-GaN.

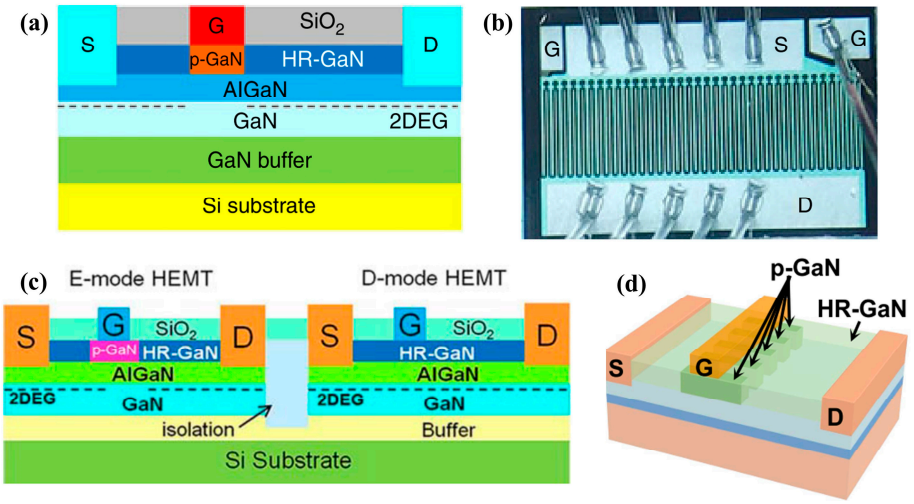

Figure 6. (**a**) A schematic cross-section and (**b**) a photograph of an HRCL-HEMT [107]. Copyright 2018, the Institution of Engineering and Technology. A schematic of the (**c**) monolithic integrated E/D-mode GaN HEMTs and (**d**) p-GaN stripe array gate E-mode GaN HEMT [108,109]. Copyright 2019, the Japan Society of Applied Physics. Copyright 2021, IEEE.

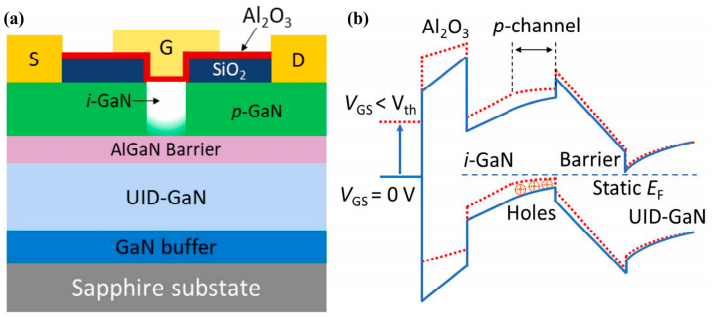

Figure 7. (**a**) A schematic of the H-treated p-Channel HEMT. (**b**) An energy band diagram of the gate region [116]. Copyright 2021, IEEE.

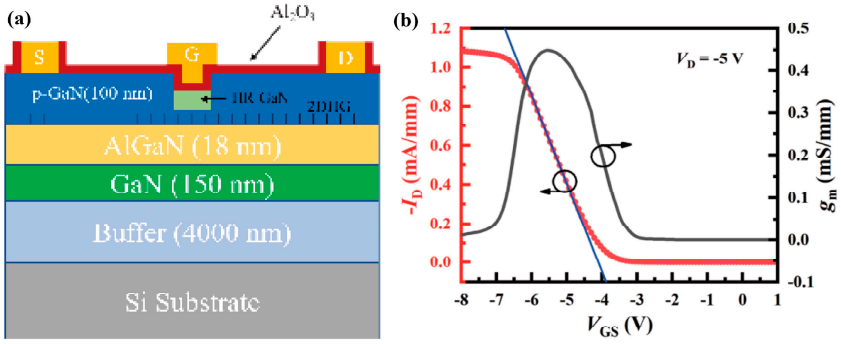

Figure 8. (**a**) Schematic of the recessed gate H-treated p-channel HFET. (**b**) Linear scale transfer characteristics [117]. Reproduced with permission from the *Journal of Semiconductors*.

In addition to the HEMTs, the fabrication of a diode is another common application area for the H Plasma treatment [118,119]. Figure 9a shows the structure of the p-GaN hybrid anode AlGaN/GaN diode (HAD) with H-treated HRCL [120]. The Mg-doped p-GaN was introduced in the anode region to regulate the on–off voltage through the doping concentration. The high-resistance GaN cap Layer structure was then obtained by self-aligning H Plasma treatment in the non-electrode region The passivation area not only restored the 2DEG but also enhanced the Electric field distribution, resulting in a high breakdown voltage exceeding 1000 V. The temperature-dependent I–V characteristics of the HAD, shown in Figure 9c, reveal a zero-temperature coefficient (ZTC) point at approximately 0.7 V. As illustrated in Figure 9b, the voltage amplitude (V_A) at a fixed current (I_A) exhibits a clear linear relationship with temperature (T) from 298 to 473 K, indicating that VA serves as an excellent temperature indicator. This temperature sensing range was further extended from 73 K to 573 K through optimization [121].

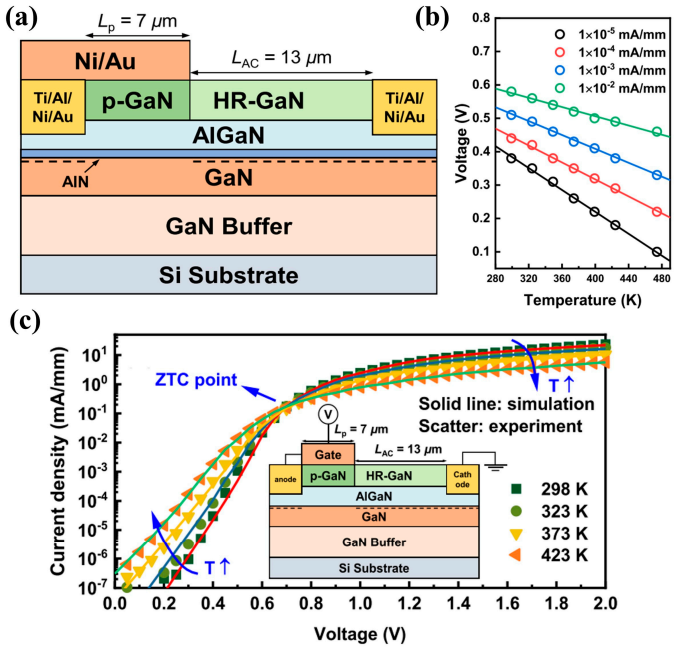

Figure 9. (**a**) A cross-section of a hybrid anode AlGaN/GaN diode. (**b**) The forward voltage against temperature with different specific current densities. (**c**) Simulation results of the forward I–V characteristics of HAD at different temperatures [120]. Copyright 2019, IEEE.

Figure 10a,b give the schematics of vertical GaN p–n diodes terminated with hydrogen ICP treatments and with mesa-etching, respectively [122]. As seen in the measurement result in Figure 10c,d, similar forward I–V characteristics, but a higher BV of 1.5 kV, were achieved in the etch-free diode compared to the mesa-terminated one. The even higher BV of 1.8 kV was reached afterward via the optimized termination of hydrogen-Plasma-based guard rings [53], whose schematics and breakdown characteristic is shown in Figure 11a,b. Additionally, a subsequent study of GaN-on-GaN p-i-n diodes proved the effectiveness of mesa and H Plasma combined termination [123]. The schematic and the Electric field distribution simulations of termination are illustrated in Figure 12a,b. The Electric field peak was shifted from the mesa edge to an inner position, resulting in the BV improvement from 375–450 V to 450–470 V at room temperature.

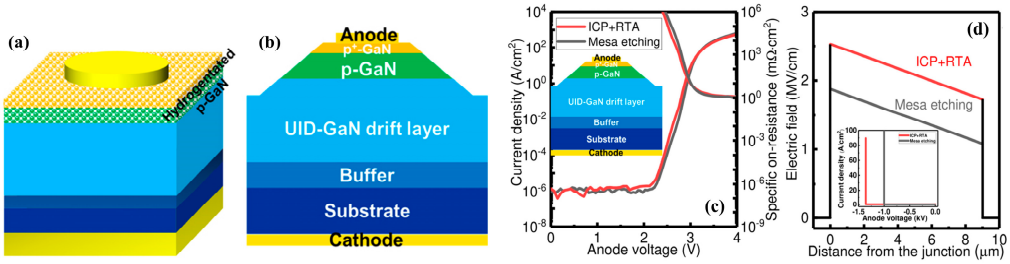

Figure 10. (**a**) Schematic diagrams of the diodes with H Plasma and RTA treatments. (**b**) A schematic of mesa-etched p–n diodes. (**c**) The forward *I*–*V* characteristics and specific on-resistance (R_{sp}) for diodes with ICP and RTA treatments, along with mesa-isolated termination. (**d**) The Electric field profiles for both devices, with the inset showing the breakdown characteristics [122]. Copyright 2019, the Japan Society of Applied Physics.

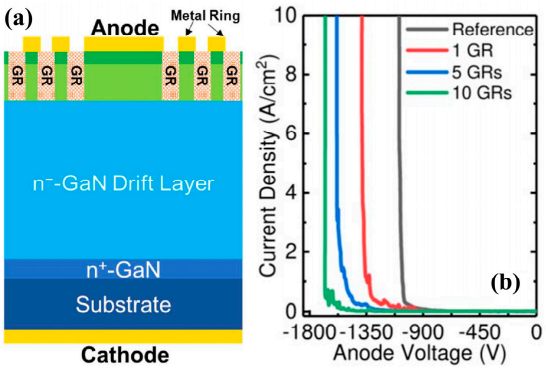

Figure 11. (**a**) The schematics of diodes with GRs. (**b**) The breakdown characteristics of the samples with different GRs [123]. Copyright 2019, IEEE.

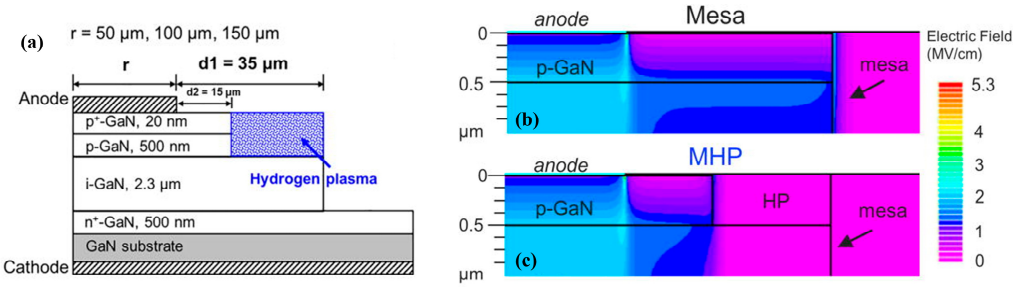

Figure 12. (**a**) A schematic representation of vertical GaN p-i-n diodes with Mesa-ET and hydrogen Plasma treatment (MHP-ET). A simulated Electric field distribution for devices with (**b**) Mesa-ET and (**c**) MHP-ET [124]. Copyright 2022, published under an exclusive license by AIP Publishing.

2.3. Summary of H Plasma Treatment

In summary, H Plasma treatment is a common technique in GaN device research. Due to the passivation effect of the H element in p-GaN, the H Plasma treatment was introduced in the p-GaN cap Layer of GaN HEMTs to recover the 2DEG in the Channel. The reverse leakage current is reduced, and the saturation current is increased after the H treatment, proving its feasibility and superiority. The application of the H Plasma technique was then further extended in areas such as E-mode p-Channel HMETs, hybrid anode AlGaN/GaN diodes, Plasma-treated termination of pin diodes, etc. With all of the progress above, H Plasma treatment has now been considered one of the most important techniques in GaN device fabrication.

3. Fluorine Plasma Treatment for GaN Electronics

3.1. The Application and Mechanism of F Plasma Treatment

Similar to the H Plasma treatment, the first application of F-Plasma treatment was also on the fabrication of E-mode GaN HEMTs [74]. The first established standard F-Plasma treatment starts with the photolithography pattern, followed by the CF_4 Plasma treatment in an RIE system at an RF Plasma power of 150 W for 150 s. However, unlike the H Plasma treatment, the F Plasma treatment here was adopted in the gate region to enhance the gate control ability. Figure 13a presents the transfer characteristics of AlGaN/GaN HEMTs before and after post-gate annealing. By defining *V*th as the gate bias at the intercept of the linear extrapolation of the drain current at the point of peak transconductance, it can be observed that true enhancement-mode operation and a *V*th shift of over 4 V were achieved through Plasma treatment.

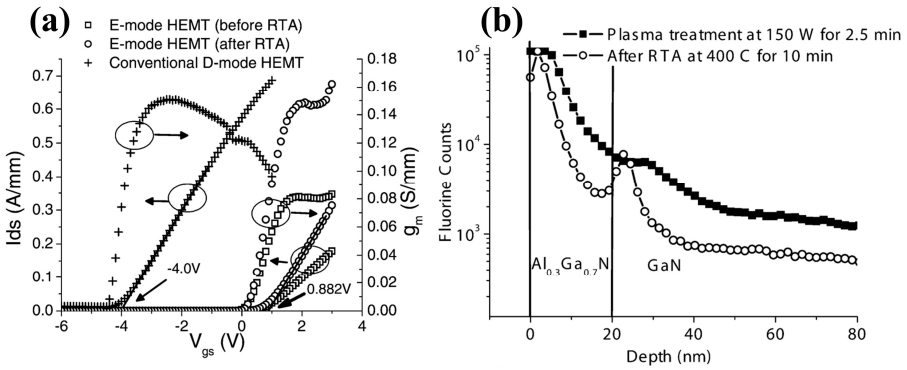

Figure 13. (**a**) Transfer characteristics of D-mode HEMTs and E-mode AlGaN/GaN HEMTs before and after rapid thermal annealing (RTA). (**b**) Concentration profiles of fluorine atoms in AlGaN/GaN samples treated with CF_4 Plasma, followed by post-gate RTA [74]. Copyright 2005, IEEE.

The mechanisms of the *V*th shift after CF_4 Plasma treatment were then investigated via secondary ion mass spectrometry (SIMS) measurements. As seen in Figure 13b, the Density of F atoms is the highest near the AlGaN/GaN interface and drops by one order of magnitude in the Channel. With these fluorine ions incorporated into the sample interface, the strong electronegativity of the fluorine ions can provide negative electric potential in the AlGaN barrier and effectively deplete the electrons in the Channel, forcing the D-mode HEMTs to be converted to E-mode. The more apparent depletion effect can be observed in the *C*-*V* measurement of the gate region [125]. Using Poisson's equation to calculate the electron Density loss, the surface barrier height must exceed 4 eV to achieve a depletion width of 100 nm. Given that GaN has a bandgap of 3.4 eV, it can be inferred that the acceptors introduced by CF_4 Plasma are responsible for the electron depletion.

For further determining the effect of F Plasma treatment, the energy level changes at ∼2.1, ∼2.8, and ∼3.25 eV were characterized by steady-state photo-capacitance spectroscopy (SSPC) techniques, which attributed to dislocations of V_{Ga}-O_N, V_{Ga}-C_N and/or C_N-O_N, and C_N, respectively [126]. Recently, the novel two-photon process was also introduced to detect the specific energy level changes in F Plasma treatment in the AlGaN/GaN heterojunctions [127]. The schematic diagram of the test device figure is shown in Figure 14a. CF_4 Plasma was introduced into the mesa via inductively coupled Plasma (ICP). During testing, two wavelengths of light were simultaneously illuminated on the device's surface. As shown in Figure 14b, a rapid increase in Ids is observed when the light wavelengths correspond to the F energy level. The detected defect energy levels at 2.8 eV and 3.25 eV below the Fermi energy of the AlGaN/GaN interface align with previous energy band characterizations [126,128].

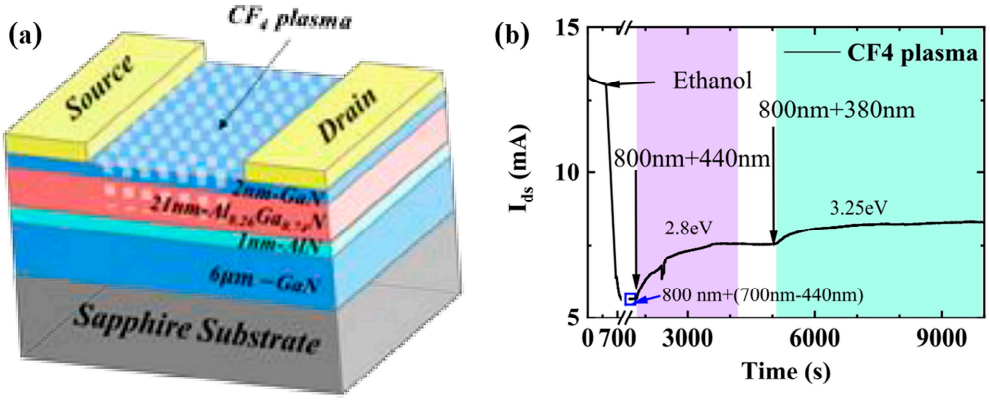

Figure 14. (**a**) AlGaN/GaN test heterostructure diagram. (**b**) Diagram of I_{ds}-t test results for CF_4 plasma-treated devices when changing spectral wavelength [127]. Copyright 2022, IEEE.

3.2. Progress of F Plasma-Treated GaN Devices

Based on the realization of the F-treated E-mode AlGaN/GaN HEMT, the integrated E/D-mode AlGaN/GaN HEMT circuit was subsequently developed [129]. As demonstrated in Figure 15a–e, a 17-stage direct-coupled field-effect transistor logic ring oscillator, developed using 1-micrometer-gate technology, functions effectively at a supply voltage of 3.5 V and achieves a minimum propagation delay of 130 picoseconds per stage. The F Plasma treatment here plays a crucial role in allowing large supply voltages in circuits, improving noise margins, and reducing gate delay. This design was further optimized by using CF_4 treatment as the device Isolation instead of the standard mesa etching technique [88]. These E/D-mode HEMTs and digital integrated circuits (ICs) fabricated using the planar process demonstrate stable operation from room temperature to 350 °C and show no signs of performance degradation after a 140-h thermal stress test, highlighting the excellent thermal stability of the process.

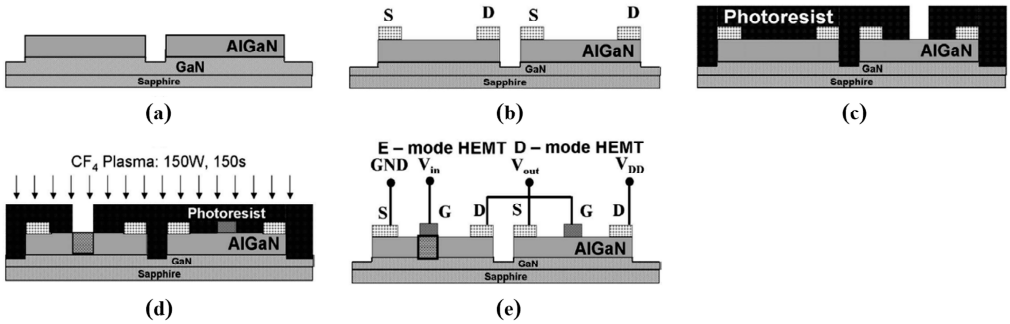

Figure 15. (**a**–**e**) The fabrication process flow of monolithic integration in E-mode and D-mode HEMTs for the inverter [129]. Copyright 2006, IEEE.

Considering the gate leakage and premature gate failure, the insulating dielectric passivation Layer was introduced in the F-treated E-mode HEMT to improve the device's stability [130]. Figure 16a–h show the fabrication process and DC characteristics of a two-step Si_3N_4 deposited F-treated E-mode HEMT. The threshold voltage has been shifted from −4 V to 2 V using the F Plasma treatment technique, and the forward turn-on gate bias reached a level as large as 7 V with the help of the two-step Si_3N_4 deposition process. A similar structure using Al_2O_3 as the gate dielectric was also studied [131], realizing a large positive threshold voltage of +3.5 V and a maximum gate input voltage of 15 V. Recently, the fluorinated graphene (FG) passivation structure on AlGaN/GaN HEMTs has been investigated [132]. As seen in the schematic in Figure 17a, the graphene on the surface was transferred using polymethyl methacrylate (PMMA). The passivation FG was then created by exposing it to F Plasma for 180 s at a bias RF power of 10 W, followed by

another passivation Layer of SiN_x, grown by Plasma-enhanced chemical vapor deposition (PECVD). The transfer characteristic exhibited in Figure 17b shows that the gate leakage current decreases four orders of magnitude after FG/SiN_x is passivated. Figure 17c shows the variation of the Schottky barrier heights among different passivated devices. The highest Schottky barrier height of 1.21 eV in the HEMT with FG passivation indicated that the reason for the decrement of the gate leakage is the enhancement of the Schottky barrier heights.

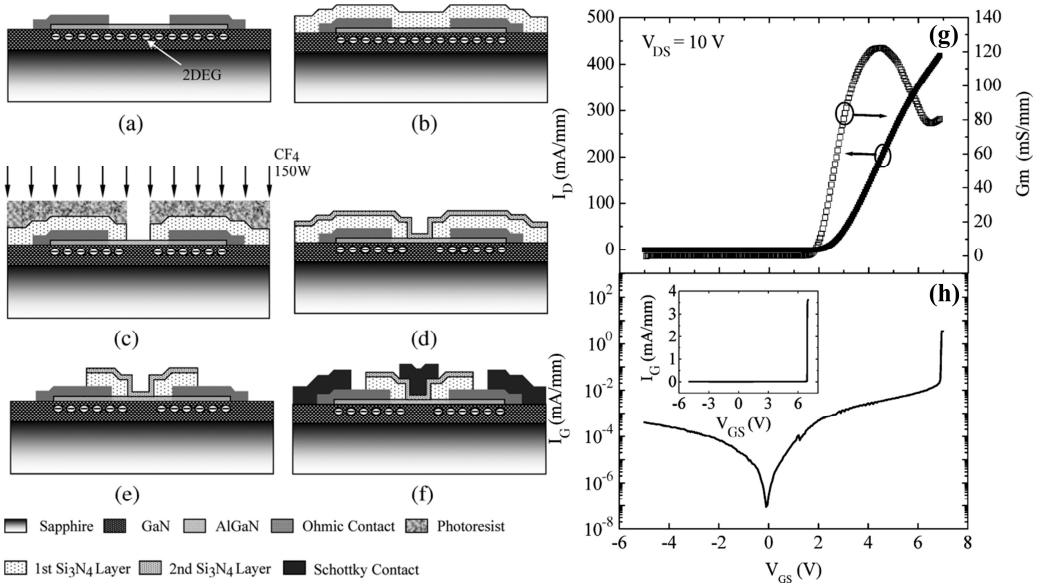

Figure 16. (**a**–**f**) Fabrication process flow of E-mode MISHFETs. (**g**) Transfer characteristics (*I-V* and G_m-*V* curve) and (**h**) gate leakage current of E-mode MISHFETs [130]. Copyright 2006, IEEE.

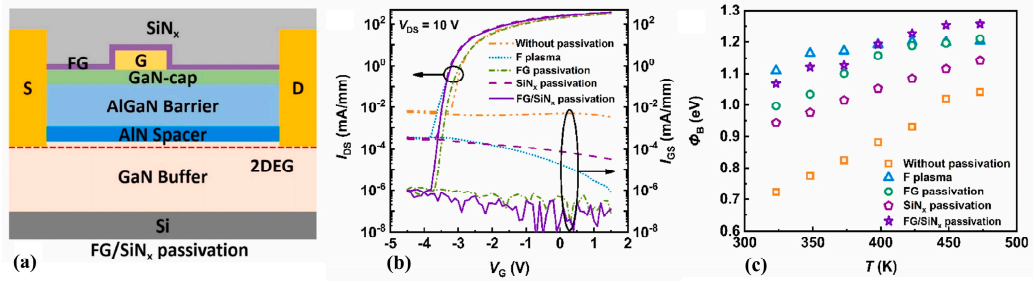

Figure 17. (**a**) Schematics of GaN HEMTs with FG/SiN_x passivation. (**b**) Transfer characteristics and (**c**) Schottky barrier heights of different treated GaN HMETs [132]. Copyright, 2023 Elsevier Ltd.

To meet the demand in improving the gate control ability and the high-frequency performance, the combination of F Plasma treatment with other gate structures has become another common design idea in GaN HEMTs. For example, the early study of the combination HEMT structure of F Plasma treatment and the recessed gate showed a current cut-off frequency (f_T) of 85 GHz and a power gain cut-off frequency (max) of 150 GHz for the small signal radiofrequency application [133]. Another E-mode GaN MIS-HEMT was designed with a partially recessed fluorine-implanted barrier [134]. After introducing the Al_2O_3 dielectric Layer and forming the MIS structure, a positive threshold voltage of +0.6 V, an ON-resistance of 7.07 Ω·mm, and a breakdown voltage of 703 V was reached while maintaining excellent thermal stability. Subsequently, the etching effect of the F Plasma treatment on the recessed region has also been studied [135]. Three devices with different gate treatments were compared together. As seen in Figure 18a,b, sample A was first treated with CF_4 RIE plasma, followed by Cl_2 ICP recess. Sample B was realized in reverse order, while sample C was only treated with Cl_2 ICP recess. The recessed region

was observed to be etched about 25 Å deeper than that of sample C, owing to the F Plasma treatment, and the device exhibits a *V*th of 1.6 V, 2.5 V, and 0.1 V for sample A, sample B, and sample C, respectively.

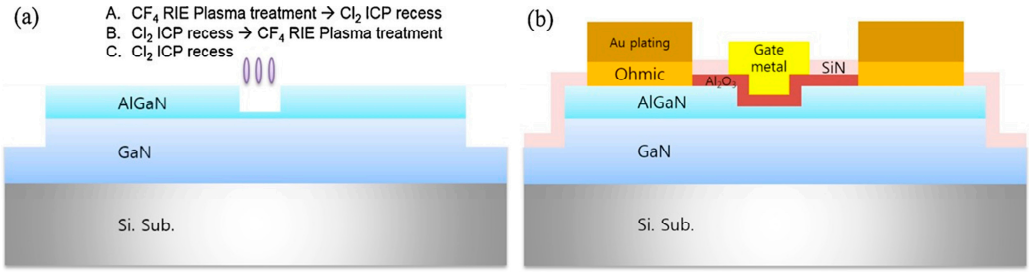

Figure 18. Schematics of (**a**) gate region treatments and (**b**) the complete F-treated GaN Metal-insulator-semiconductor HEMT (MISHEMT) [135]. Copyright 2015, WILEY-VCH Verlag GmbH & Co. KGaA, Weinheim, Germany.

Additionally, to realize the deep-treated technique under the gate region, the study of two-step fluorine treatment is also worth mentioning [136]. In this study, the sample was initially treated with CF_4 Plasma at an RF power of 120 W for 100 s and then annealed at 600 °C for 10 min after opening the gate dielectric. The combination of high RF power and elevated Annealing Temperature allowed the peak concentration of implanted F^- ions in the GaN Buffer to diffuse to greater depths. A second CF_4 Plasma treatment was applied at an RF power of 80 W for 80 s after defining the gate foot using electron beam lithography. SIMS measurements indicated that the Density of immobile negatively charged F^- ions in the two-step F-treated device was higher than that in the one-step treatment, both in the AlGaN barrier and the GaN Buffer. This higher Density of immobile negative charge can cause a larger upward bending of the conduction band and yield a higher barrier height in the gate region. The transfer characteristic demonstrates the normally-off performance of the device, and the breakdown voltage is also increased.

As one of the important application areas of GaN HEMTs, F Plasma treatment is also widely used in detector fabrication to improve performance. Figure 19a is the schematic diagram of the ungated HEMTs with CF_4 Plasma treatment [137]. The Plasma treatment was conducted at an RF power of 30 W for 2 min. For the polar gas test, the samples were placed in a chamber where polar liquids were added along the sidewalls and allowed to naturally volatilize, filling the chamber. The results are illustrated in Figure 19b,c. For the sample without F Plasma treatment, the currents decreased by approximately 1.9 mA (16%), 2.2 mA (17%), and 2.7 mA (19%). In contrast, the currents of the BL sample treated with F Plasma decreased by 2.6 mA (54%), 4.1 mA (61%), and 4.17 mA (63%) in the presence of ethanol, acetic acid, and acetonitrile, respectively. Figure 20a–d provide a mechanistic explanation for these phenomena. When polar liquids were applied to the AlGaN surface, they dissolved the positive ions, disrupting the coupling between surface negative polarization charges and positive ions, as well as the interactions between F^- charges and surface positive ions [138,139]. Because the dipole moment of the F^- charges interacting with surface positive ions is considerably larger than that of the surface negative polarization charges with the same positive ions, the surface positive ions in the F-treated AlGaN/GaN heterojunction dissolve more easily. The removal of these surface positive ions leads to a proportional decrease in the number of electrons in the Channel, ensuring electric neutrality is maintained.

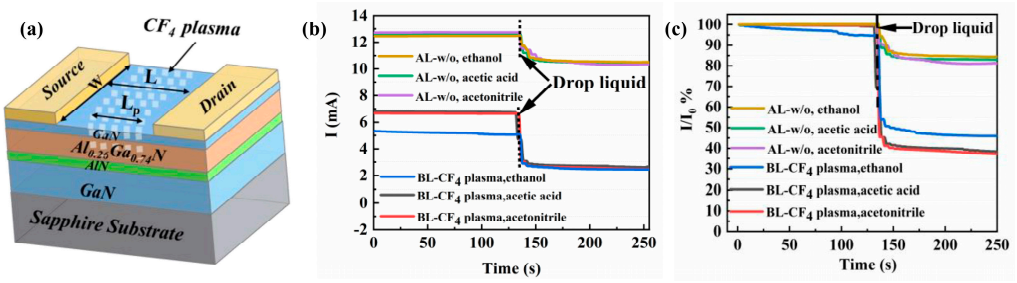

Figure 19. (**a**) A schematic diagram of the ungated HEMTs with CF_4 Plasma treatment. (**b**) The I-t curves affected by polar liquids. (**c**) The normalized I-t curves affected by polar liquids [137]. Copyright 2023, by the authors. Licensee: MDPI, Basel, Switzerland.

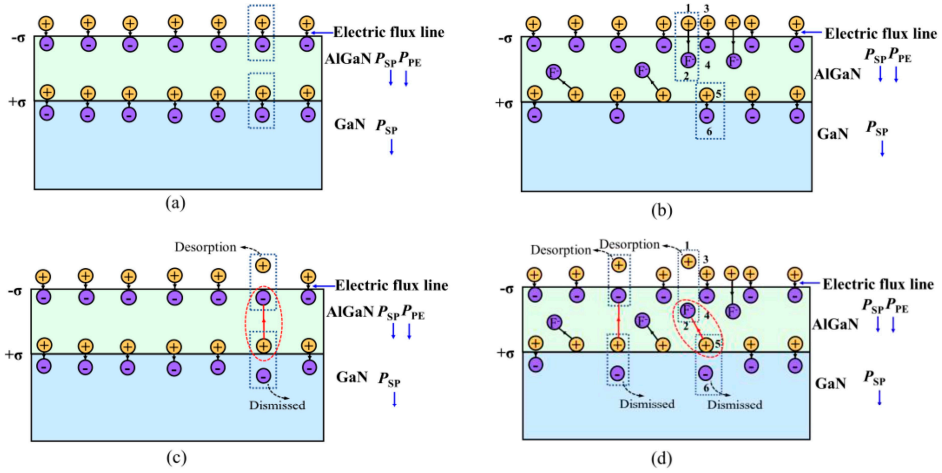

Figure 20. Physical model diagrams of the surface of AlGaN/GaN devices, (**a**) without Plasma treatment, (**b**) with CF_4 Plasma treatment, (**c**) without Plasma treatment being affected by polar molecules, and (**d**) with CF_4 Plasma treatment being affected by polar molecules [137]. Copyright 2023, by the authors. Licensee: MDPI, Basel, Switzerland.

The GaN HEMTs schematic fabricated by Song et al. is an early example of F-treated device termination [140]. An extra CF_4 Plasma treatment with an RF power of 150 W masked by photolithography was applied for 45 s to form a low-Density drain (LDD) area near the gate region. It is reported that the breakdown voltage was improved by 50%, and the current collapse was reduced in LDD-HEMTs. Such passivated termination was then adopted in the research of GaN SBDs. As seen in the schematic in Figure 21a, the post-etching F Plasma treatment was introduced using CF_4 in the ICP system for 120 s [141]. The subsequent measurement showed that the forward current (I_{FOR}) increased by 27%, and the significant reverse current (I_{REV}) decreased after the F Plasma treatment, as seen in Figure 21b,c. The main reason for the great improvement of forward characteristics is that the F Plasma treatment suppresses electrons transporting through the anode sidewall and forces more electrons to flow through the 2DEG Channel. Besides, the acceptor traps produced by the F Plasma also contribute to the suppression of I_{REV}.

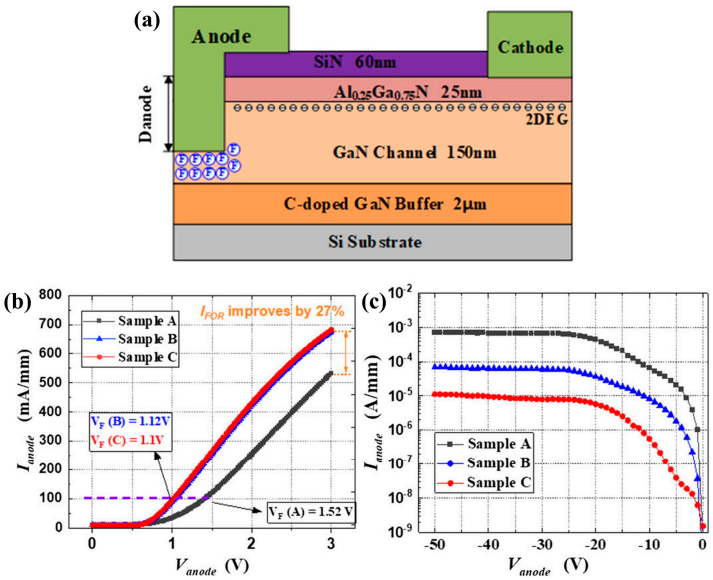

Figure 21. (**a**) A cross-sectional view of the deep recessed anode SBDs with F Plasma treatment. (**b**) The forward and (**c**) reverse I–V characteristics of the three samples [142]. Copyright 2021, Wiley-VCH GmbH.

3.3. Enhanced Device Performance via F Ion Implantation

Even though F Plasma treatment via ICP devices has become a common process in GaN device fabrication, the standard equipment is difficult to establish due to the variety of Plasma-generating devices [143,144]. As for the ion implantation method, the depth and concentration of ions can be accurately controlled by regulating the energy and dose, showing high reliability and repeatability [145–147]. Thus, replacing the Plasma treatment technique with ion implantation can be an effective option to meet the mass production requirement. The early application of F ion implantation in GaN HEMTs was intended to solve the source electron injection into the gate Buffer Layer [148]. The gate area of the HEMTs was implanted by $^{19}F^{+}$ ions with an energy of 50 keV at a dose of 1×10^{12} cm^{-2}. The high resistivity area formed by fluorine ions blocks the source-injected electrons and avoids the peak Electric field in the gate region, thus preventing the premature breakdown of the devices. Another example of an E-mode GaN HEMT was formed by F ion implantation with an energy of 25 keV at a dose of 6×10^{12} cm^2 into the gate region, with the Si_3N_4 serving as the sacrificing Layer [149]. The significant shift of *V*th from negative to positive was reached, and its reason is deduced to be related to the negatively charged fluorine ions in AlGaN/GaN heterojunction, which is a similar mechanism as the one found in F Plasma-treated GaN HEMTs.

Based on the standard F ion implantation process, the device performance was further improved by fabricating GaN MIS-HEMTs. As seen in the device schematic in Figure 22a, an 8 nm Si_3N_4 Layer was deposited via low-temperature chemical vapor deposition (LPCVD) as a gate insulator and energy-absorbing Layer [150]. It has been reported that the Plasma-free LPCVD technique can produce Si_3N_4 films with superior quality and enhanced thermal stability at higher deposition temperatures compared to PECVD and ICP-CVD methods. Additionally, the Si_3N_4 gate dielectric functioned as an energy-absorbing Layer, which slowed down high-energy fluorine ions, allowing them to be incorporated into the barrier rather than the Channel region. Figure 22b,c demonstrate the transfer characteristic of the MIS-MEMT in linear and semi-log scales, respectively. The high threshold voltage of 3.3 V was observed, as well as the low hysteresis and high on/off ratio of 4×10^9. With these achievements in F ion implanted E-mode HEMTs, the two-terminal terahertz detectors can be fabricated in a large array of antenna-coupled GaN HEMTs, and the schematic is shown in Figure 23a,b [151]. An antenna-coupled HEMT detector operating as a two-terminal

terahertz rectifier reached a noise equivalent power of 47 pW/ $\sqrt{}$Hz at 0.65 THz with an optimal ion dosage of about 1.6×10^{13} cm^2.

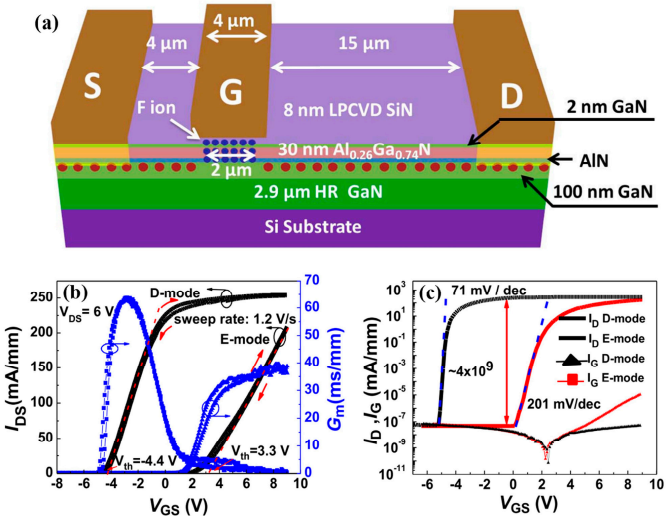

Figure 22. (**a**) A schematic of AlGaN/GaN MIS-HEMTs. (**b**) The transfer curves of the devices at V_{DS} of 6 V in linear scale. (**c**) The transfer curves together with the I_g in a semi-log scale [150]. Copyright 2015, IEEE.

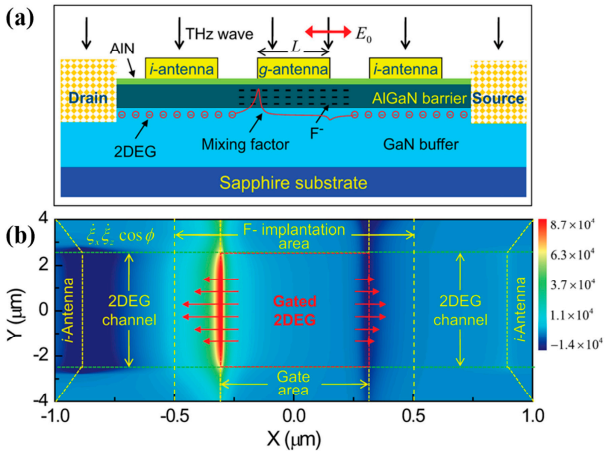

Figure 23. (**a**) A cross-section of the HEMT terahertz detector. (**b**) A color-scale 2D plot of the spatial distribution of the mixing factor [151]. Copyright 2019, and published under license by AIP Publishing.

In the ion implantation process, even though thermal annealing is mostly applied to repair the damage, the degradation of crystal quality is inevitable, causing the decrease of Channel mobility and saturation current in the devices [152–154]. Recently, a doping method utilizing the porous AlF_3 material has been invented [155]. It was discovered that the AlF_3 could be chemically bonded to the H_2O attached to the porous structure and then develop a possible mechanism of a displacement reaction at a high temperature to form the free F ions. This phenomenon makes $AlF_3 \cdot 3H_2O$ a suitable fluorine ion source for ion thermal diffusion experiments. Figure 24a–d depicts the fabrication process of an F ion diffused GaN HEMT. A 50 nm AlF_3 film and a cap Layer of a 100 nm SiO_2 were grown by thermal evaporation and PECVD, respectively. The samples were then annealed at 800 °C for 2 h in an N_2 atmosphere, followed by the movement of the AlF_3 and SiO_2 through BOE wet etching. As seen in the transfer characteristic in Figure 24e, the positive *V*th of 1.8 V was achieved after the F ion diffusion. The comparison of the *V*th shift between different

F-treated HEMTs is also carried out in Figure 24f. The greatest *V*th stability of F ion diffused devices demonstrates that fewer defects were induced through the ion diffusion method.

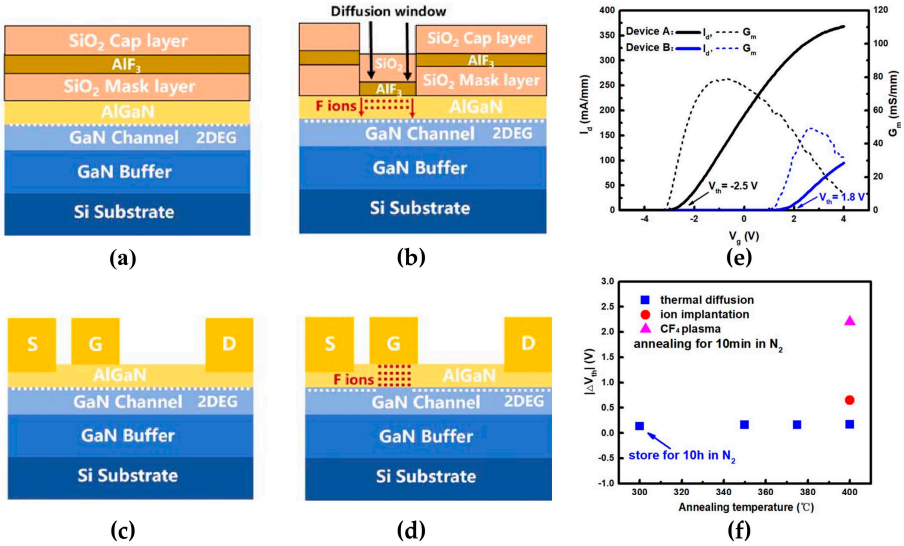

Figure 24. A schematic diagram of thermal diffusion F doping structure of (**a**) device A and (**b**) device B, (**c**) device A, and (**d**) device B. (**e**) The transfer characteristic of the devices A and B. (**f**) *V*th shift of a fluorine-based E-mode HEMT [155]. Copyright 2019, the Japan Society of Applied Physics.

3.4. Summary of F Plasma Treatment

In summary, F Plasma treatment is another common technique for GaN device fabrication. The first application of F Plasma in E-mode GaN HEMTs revealed that the extra electric potential was introduced by the negative fixed F^- ion instead of the doping characteristic. Subsequently, several signs of progress have been made in the F-treated devices, such as fluorinated graphene passivation, two-step F Plasma treatment, low-Density drain termination, etc. Moreover, the F ion implantation was also applied to solve the instability of ICP Plasma treatment, bringing specific depth and Density of F ion in the GaN devices.

4. Other Plasma Treatments for GaN HEMTs

4.1. N Plasma Treatment for GaN Electronics

To solve the interface state problem in the GaN MIS-HEMTs, the in situ, remote Plasma pretreatment (RPP) process was developed. For example, Yang et al. designed the gate stack treated by in situ low-damage RPP [156]. Before depositing the Al_2O_3 dielectric, the gate regions were treated with an $NH_3/Ar/N_2$ (2/5/20 min) Plasma in a Plasma-enhanced ALD system, applying an RF Plasma power of 50 W and maintaining the Substrate at 300 °C. The NH_3-Ar Plasma effectively eliminated the native oxide Layer, while the N_2 Plasma facilitated nitridation, resulting in the formation of a nitridation interLayer (NIL) on the III-N surface. The optimized in situ Plasma nitridation creates a thin Layer of NIL that acts as an effective oxygen barrier, inhibiting the formation of Ga-O bonds during the subsequent Al_2O_3 deposition. This leads to a uniform and sharp interface between Al_2O_3 and the GaN cap. As demonstrated in the transfer and output characteristics of MIS-HEMTs with and without RPP, the *V*th hysteresis was significantly reduced from 1.4 V to 0.09 V after the Plasma treatment. This in situ nitridation process was subsequently introduced before the Si_3N_4 deposition for the GaN MIS-HEMT fabrication [157]. As seen in the device schematic in Figure 25a, an in situ Plasma nitridation process was performed in a reformed LPCVD system using pure N_2 gas at an RF power of 50 W and a pressure of 300 mTorr at 400 °C for 3 min. An even further significant *V*th shift decrease from 5.23 V to 0.27 V was Extracted from the measured transfer curves in Figure 25b,c, further proving the feasibility of N Plasma treatment on eliminating interface states.

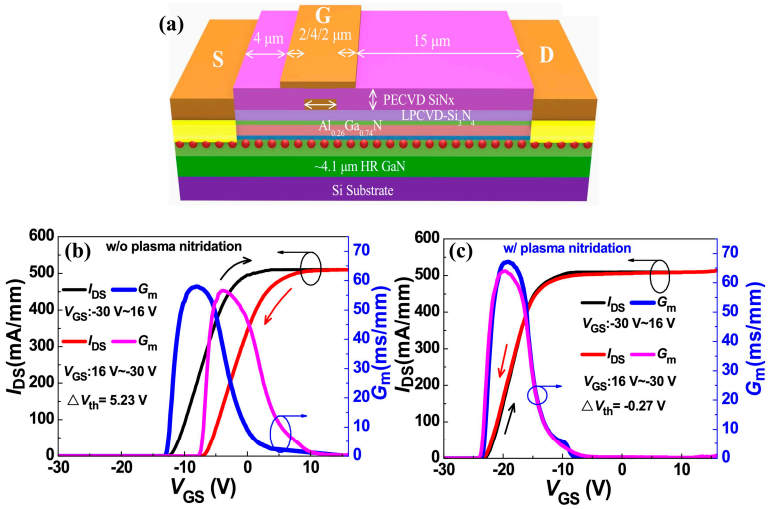

Figure 25. (**a**) Schematic of AlGaN/GaN MIS-HEMTs with Si_3N_4 as gate dielectric. Transfer curves (**b**) without and (**c**) with in situ pre-deposition Plasma nitridation. The colored arrows indicate the forward and reverse progression along the curve. [157]. Copyright 2016, IEEE.

Through studying the passivation effect of N Plasma treatment on p-GaN, the N-treated E-mode GaN HEMT, similar to H-treated devices, was developed [158]. As seen in Figure 26a,b, the normally-off device was manufactured via self-aligned nitrogen Plasma treatment through ICP processing at room temperature for 5 min, while the radio frequency (RF) power, ICP power, and pressure were set as 80 W, 500 W, and 15 mTorr, respectively. The XPS valence band spectra measurements presented in Figure 26c indicate that the surface valence band shifted from 0.8 eV to 2.3 eV following Plasma nitridation. Additionally, the surface Fermi level in the p-GaN after nitrogen Plasma treatment shifted toward the conduction band by 1.5 eV, resulting in the conduction band being lowered below the Fermi level and facilitating the recovery of the 2DEG. The obvious normally-off operation and positive *V*th of 1.1 V can be Extracted from the transfer characteristics in Figure 26d,e, and the high breakdown voltage of 1215 V also benefited from the passivation effect.

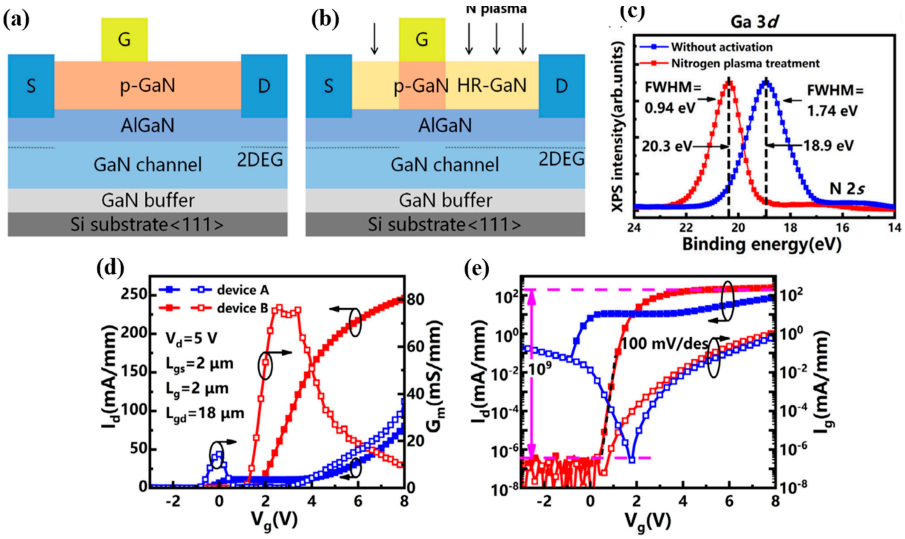

Figure 26. Schematic of GaN HEMT with different processes: (**a**) device A as-grown and (**b**) device B with nitrogen Plasma treatment. (**c**) Ga 3d core-level spectra without and with nitrogen Plasma treatment. Transfer and transconductance characteristics of device A and device B in (**d**) linear and (**e**) log scale [158]. Copyright 2023, Wiley-VCH GmbH.

4.2. O Plasma Treatment for GaN Electronics

In the early study of doping characteristics in gallium nitride, the presence of O in insulating Mg-doped GaN was discovered by photoconductivity experiments, and the existence of Mg-O complexes was also verified by ultraviolet reflection spectrometry [159,160]. Based on this mechanism, it could be feasible to make Plasma oxidated E-mode GaN HEMTs following the method of an H-treated device. Figure 27a,b show the schematic of as-grown (device A) and O-treated (device B) GaN HEMTs [161]. After the gate metal deposition, device B was treated with an optimized self-aligned oxygen Plasma passivation process, followed by rapid thermal annealing (RTA) at 350 °C for 5 min to address any Plasma-induced damage. The transfer characteristics of both devices A and B are depicted in Figure 27c,d. Featuring a p-GaN gate structure, device B achieved a threshold voltage (V_{TH}) of 1.02 V at a drain current of 10 μA/mm. Furthermore, the maximum drain current Density and peak transconductance for device B increased to 301 mA/mm and 63 mS/mm, respectively, marking a 3.5-fold and 2.4-fold enhancement compared to device A. Furthermore, the significant increase of BV from 15 V to 660 V after oxygen Plasma treatment shows the potential of O Plasma treatment for power switching applications. Additionally, in the E-mode AlON/AlN/GaN HEMTs fabricated by Liu et al., the AlN Layer was also oxidized by O_2 Plasma at 200 W power for 20 min, producing a device with a breakdown voltage of 74 V and threshold voltage of 0.4 V.

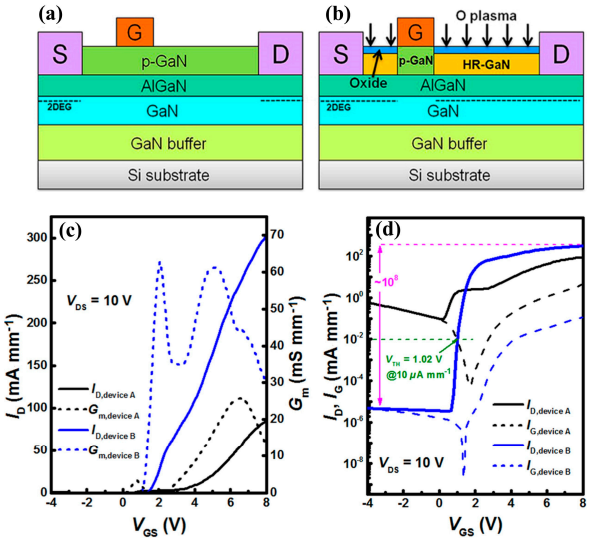

Figure 27. Schematic diagram of (**a**) as-grown (device A) and (**b**) oxygen Plasma-treated GaN HEMT (device B). Transfer characteristics of device A and device B in (**c**) linear and (**d**) log coordinates [161]. Copyright 2019, the Japan Society of Applied Physics.

During the research of GaN devices, several elements were applied in the surface Plasma treatment to passivate the interface states, and oxygen is no exception. In a study on $HfO_2/Al_2O_3/AlN$ stacked structures, in situ remote Plasma pretreatments with O_2, NH_3, and NH_3–O_2 were carried out and compared [162]. As seen in the D_{it} estimation in GaN MIS diodes with various RPPs Extracted from frequency-dependent C–V measurement, the D_{it} was remarkably reduced by two orders of magnitude via NH_3 RPP, while the decrease by only one order of magnitude was reached using O_2 RPP. The XPS spectra of Ga 3d core-level further revealed the mechanism of discrepancies. The sample without RPP showed a much higher Ga_2O content of 54.4% than the other three samples. Combined with the D_{it} calculation, it can be concluded that the content of Ga_2O has a strong positive correlation with the interface traps. In the NH_3 treated sample, the Ga–N concentration increased remarkably due to the reaction between Ga_2O and NH_3, resulting in the high-quality dielectric/GaN interfaces. As for the sample with O_2 RPP, the rise in Ga_2O_3/GaN was a direct result of the oxidation, and the D_{it} only slightly deteriorated.

4.3. Comparison Between Different Plasma Treatment

The analysis above reveals that most of the Plasma treatment technologies have a similar effect on passivation. Taking E-mode GaN HEMTs as an example, the H, O, and N Plasma were all employed to treat the p-GaN cap Layer to restore the 2DEG in the Channel by passivating the Mg acceptors, resulting in the formation of complexes between the treatment elements and the acceptors, such as Mg-H and Mg-O [90,163]. Typically, these Plasma treatments are performed using the ICP tools. Table 2 presents a comparison of key parameters for the ICP tools used in various Plasma treatments on GaN HEMTs, specifically for the 70 nm thick p-GaN Layer. A notable difference is observed in the RF power, as the H Plasma process operates at a significantly lower power (2–10 W) compared to other treatments (80–90 W). This discrepancy can be qualitatively attributed to the atomic size, as the hydrogen atom is much smaller than oxygen and nitrogen atoms, thus requiring less RF power to penetrate to the desired depth [90]. As for F Plasma treatment, the mechanism of forming fixed negative interface charges is quite different from the other Plasma techniques. It is applied to the AlGaN Layer under the gate rather than the p-GaN cap Layer between the three electrodes.

Table 2. Comparison of operation parameters of different Plasma treatments to p-GaN [73,158,161].

Plasma Type	RF Power (W)	ICP Power (W)	Pressure (mTorr)	Time (min)
Hydrogen	2–10	300	8	1–10
Nitrogen	80	500	15	5
Oxygen	90	500	-	-

To further compare the effects of various Plasma treatments, the performance of several E-mode Plasma-treated GaN HEMTs is analyzed. These devices have similar dimensions and structures, allowing for a direct comparison. As shown in Table 3, devices treated with N Plasma exhibit a higher on/off ratio and breakdown voltage compared to those treated with other Plasmas. This result indicates that the N Plasma treatment can passivate the p-GaN Layer more effectively, reducing gate leakage current and enhancing breakdown voltage endurance in the gate-to-drain region. This effect may also be attributed to the crystal structure restoration afforded by N Plasma treatment, along with a subsequent annealing process. Studies have shown that N Plasma can help restore atomic order within the GaN crystal structure, reducing bulk defects after appropriate heating. Additionally, it can shift the p-type GaN film toward slight n-type conductivity, which promotes Electric field redistribution in the HEMT Channel Layer. In contrast, devices treated with H Plasma show higher Vth and I_{sat} than those treated with other Plasmas, indicating an efficient Mg-H complex formation.

Table 3. A comparison of the performance of E-mode HEMTs treated by different Plasma [73,150,158,161].

Treatment Mechanism	Treatment to p-GaN; Except Gate Region			Treatment to AlGaN; Only Gate Region
Plasma type	H	N	O	F
$L_{GS}/L_G/L_{GD}$ (μm)	5/2/11	2/2/18	4/4/15	4/4/15
Vth (V)	1.75	1.1	1.02	0.92
On/Off ratio	10^7	10^9	10^8	10^9
I_{sat} at V_{GS} = 8 V (mA/mm)	320	245	300	205
BV (V)	567	1215	660	573
ΔVth at 200 °C (mV)	−100	−200	−150	−500

Since Plasma treatment often introduces unavoidable damage and defects, it is essential to evaluate the stability of Plasma-treated devices. In particular, the Vth shift of −200 mV at 200 °C is observed in the N Plasma-treated HEMTs, while devices treated

with H Plasma, a more established technology, demonstrate relatively more stable thermal performance, with a ΔV_{th} of −100 mV. The minimal threshold voltage shift suggests that the Plasma-induced complexes (Mg-H, Mg-N, and Mg-O) exhibit excellent thermal stability. As for F Plasma treatment by ICP, we can expect fixed charges and more interface states to be introduced to the gate region at the same time. However, seldom reports can be found about its thermal stability. As for F treatment by ion implantation, the *V*th shift is around 500 mV, as reported.

For further comparison, Figure 28a,b illustrate the differences in *V*th and on/off ratio, respectively. As shown in Figure 28a, the F-treated GaN HEMTs exhibit a wide range of *V*th variability, demonstrating their capacity to fine-tune the threshold voltage by modulating the fixed charge concentration. In contrast, the H-treated devices show a more limited Vth adjustment. The effects of N and O treatments remain unclear due to the scarcity of reported data. In the on/off ratio comparison, the F-treated devices achieve a high value of up to 10^{10}, also likely due to the additional negative potential from F^- charges, which helps to reduce reverse leakage current. Figure 28c presents the breakdown voltage (BV) and specific on-resistance ($R_{on,sp}$) benchmarks for E-mode GaN HEMTs with different Plasma treatments. The equations for calculating the Baliga figure of merit (BFOM) of vertical devices and lateral GaN HEMTs are exhibited below as follows [164]:

$$R_{ON,SP} = \frac{4BV^2}{\varepsilon_s \mu E_C^3} \tag{3}$$

$$BFOM = \varepsilon_s \mu E_C^3 \tag{4}$$

$$R_{ON,SP}(HEMT) = \frac{BV^2}{q\mu Q_s E_C^2} \tag{5}$$

$$BFOM(HEMT) = q\mu Q_s E_C^2 \tag{6}$$

where ε_s, q, μ, Q_s, and E_c represent the dielectric constant, electron charge (1.6×10^{-19} C), electron mobility in GaN (1250 $cm^2V^{-1}s^{-1}$ for vertical; 2000 $cm^2V^{-1}s^{-1}$ for HEMT), sheet carrier Density (1×10^{13} cm^{-3}), and critical Electric field (3.3 $MVcm^{-1}$), respectively.

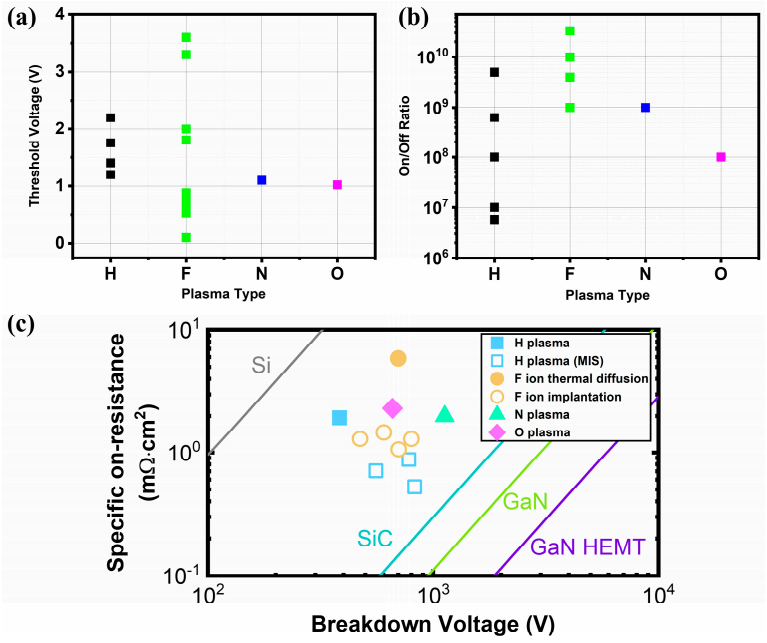

Figure 28. Comparison of (**a**) *V*th and (**b**) on/off ratio among different Plasma-treated GaN HEMTs. (**c**) BV and $R_{on,sp}$ benchmark of E-mode GaN HEMTs with different Plasma treatments [73,74,89,104–106,108,129,133,134,150,155,158,161,165–167].

5. Conclusions

In conclusion, Plasma treatment technologies have been widely utilized in the fabrication of GaN electronic devices and have achieved considerable improvements. Developed from the p-type doping research for GaN: Mg, the H Plasma treatment is introduced to passivate the p-GaN Layer of p-GaN gate HEMTs to restore the 2DEG in the Channel for replacing the etching process, reaching a typical threshold voltage (Vth), saturation current, and transconductance of 1.75 V, 188 mA/mm, and 73.1 mS/mm, respectively. Based on this reliable treatment technique, designs such as the DCFL system, p-GaN stripe array gate, E-mode p-Channel HEMT, and p-GaN diode with high breakdown voltage are established, fully proving the feasibility and reliability of this technology. F Plasma treatment is another common technique in GaN devices. The negative electric potential can be introduced in the CF_4 Plasma-treated gate region to deplete the Channel, transforming the D-mode GaN HEMTs to E-mode. Combined with gate dielectric, recessed etching, and extra F Plasma treatment process, the reliability and performance of F-treated normally-off GaN HEMTs have been significantly improved. Furthermore, the F Plasma treatment is also applied in the termination of GaN HEMTs and diodes, boosting the forward current by 27% in the diodes. Other Plasma treatment techniques developed recently, such as N Plasma and O Plasma, are successively established, expanding the range of options for Plasma treatment in GaN device fabrication. Regarding thermal stability, implementing a dielectric passivation Layer alongside an annealing process has proven effective. This method helps eliminate interface states and improves the on/off ratio in many Plasma-treated devices.

Overall, considering the progress and challenges in Plasma treatments for GaN HEMTs, we propose several perspectives for future research:

1. The main challenge in Plasma treatment technology lies in ensuring the reliability and stability of its effects. Several other factors, such as defect Density in the epitaxial Layers, can also impact the treatment outcomes. However, there is currently no research addressing the influence of these defects, which could be a valuable research project in the future for Plasma treatment in GaN.
2. Ion implantation offers a more precise alternative to Plasma treatment for introducing elements like H, N, O, and F. The effectiveness of this method has already been demonstrated with F ion implantation, making it a promising avenue to explore for H, N, and O treatments, as well.
3. Nitrogen and oxygen Plasma treatments, as emerging techniques, have shown promising passivation effects in p-GaN gate HEMTs, indicating a strong potential for further development. However, additional research is required to fully understand and optimize their applications.
4. H and N Plasma treatments have shown distinct advantages in improving the BFOM of p-GaN gate HEMTs: H Plasma effectively reduces on-resistance, while N Plasma decreases leakage current. A combined H and N Plasma treatment could potentially harness these complementary benefits, driving GaN HEMT performance closer to its material limits.

Author Contributions: Conceptualization, Y.C., B.Z. and K.F.; writing—original draft preparation, B.L. and I.R.; writing—review and editing, I.R., H.D.E., H.F., Y.Z. and Y.C.; supervision, H.F., Y.Z., Y.C., B.Z. and K.F. All authors have read and agreed to the published version of the manuscript.

Funding: This research was funded by the support of ULTRA, an Energy Frontier Research Center funded by the U.S. Department of Energy, Office of Science, Basic Energy Sciences under Award # DE-SC0021230, the University of Utah start-up fund, and PIVOT Energy Accelerator Grant U 7352FuEnergyAccelerator2023. This work was also supported, in part, by Applied Materials, by CHIMES, one of the Seven Centers in JUMP 2.0, a Semiconductor Research Corporation (SRC) Program by DARPA, and by the Key Research and Development Program of Jiangsu Province (No. BE2022057-1) and the Key Research and Development Program of Jiangxi Province (No. 20223BBE51033).

Institutional Review Board Statement: Not applicable.

Informed Consent Statement: Not applicable.

Data Availability Statement: The data presented in this study are available on request from the corresponding author.

Conflicts of Interest: The authors declare no conflicts of interest.

References

1. She, X.; Huang, A.Q.; Lucía, O.; Ozpineci, B. Review of Silicon Carbide Power Devices and Their Applications. *IEEE Trans. Ind. Electron.* **2017**, *64*, 8193–8205. [CrossRef]
2. Yablonovitch, E.; Jiang, H.; Kosaka, H.; Robinson, H.D.; Rao, D.S.; Szkopek, T. Optoelectronic quantum telecommunications based on spins in semiconductors. *Proc. IEEE* **2003**, *91*, 761–780. [CrossRef]
3. Gutiérrez-Castrejón, R.; Duelk, M.; Bianco, S. Modeling and simulation of semiconductor optical amplifier dynamics for telecommunication applications. In *Computer Physics Research Trends*; Nova Science Publishers: New York, NY, USA, 2007; pp. 89–124.
4. Tillman, J. The expanding role of semiconductor devices in telecommunications. *Radio Electron. Eng.* **1973**, *43*, 82–90. [CrossRef]
5. Johnson, C.M. Current state-of-the-art and future prospects for power semiconductor devices in power transmission and distribution applications. *Int. J. Electron.* **2003**, *90*, 667–693. [CrossRef]
6. Qiu, J.; Liu, K.; Wu, Y. A pulsed power supply based on power semiconductor switches and transmission line transformer. *IEEE Trans. Dielectr. Electr. Insul.* **2007**, *14*, 927–930. [CrossRef]
7. Wang, B.; Cai, J.; Du, X.; Zhou, L. Review of power semiconductor device reliability for power converters. *CPSS Trans. Power Electron. Appl.* **2017**, *2*, 101–117. [CrossRef]
8. Liou, K.-Y.; Raybon, G. Operation of an LED with a single-mode semiconductor amplifier as a broad-band 1.3-μm transmitter source. *IEEE Photonics Technol. Lett.* **1995**, *7*, 1025–1027. [CrossRef]
9. Shields, A.J. Semiconductor quantum light sources. *Nat. Photonics* **2007**, *1*, 215–223. [CrossRef]
10. Jandt, K.D.; Mills, R.W. A brief history of LED photopolymerization. *Dent. Mater.* **2013**, *29*, 605–617. [CrossRef] [PubMed]
11. Hamada, K. Present status and future prospects for electronics in electric vehicles/hybrid electric vehicles and expectations for wide-bandgap semiconductor devices. *Phys. Status Solidi* **2008**, *245*, 1223–1231. [CrossRef]
12. Liu, Y.Q.; Li, Y.J.; Wu, Y.L.; Yang, G.T.; Mazzarella, L.; Procel-Moya, P.; Tamboli, A.C.; Weber, K.; Boccard, M.; Isabella, O.; et al. High-Efficiency Silicon Heterojunction Solar Cells: Materials, Devices and Applications. *Mater. Sci. Eng. R-Rep.* **2020**, *142*, 100579. [CrossRef]
13. Kawahashi, A. A new-generation hybrid electric vehicle and its supporting power semiconductor devices. In Proceedings of the 16th International Symposium on Power Semiconductor Devices and ICs, Kitakyushu, Japan, 24–27 May 2004; pp. 23–29.
14. Bose, B.K. Power electronics and motor drives recent progress and perspective. *IEEE Trans. Ind. Electron.* **2008**, *56*, 581–588. [CrossRef]
15. Bose, B.K. Power electronics and motor drives-recent technology advances. In Proceedings of the IEEE International Symposium on Industrial Electronics (ISIE), L'Aquila, Italy, 8–11 July 2002; pp. 22–25.
16. Wilamowski, B.M.; Irwin, J.D. *Power Electronics and Motor Drives*; CRC Press: Boca Raton, FL, USA, 2018.
17. Batra, G.; Jacobson, Z.; Madhav, S.; Queirolo, A.; Santhanam, N. *Artificial-Intelligence Hardware: New Opportunities for Semiconductor Companies*; McKinsey and Company: New York City, NY, USA, 2019; Volume 2.
18. Zhang, S.; Xue, X.; Tangdiongga, E.; Calabretta, N. Low-latency optical wireless data-center networks using nanoseconds semiconductor-based wavelength selectors and arrayed waveguide grating router. *Photonics* **2022**, *9*, 203. [CrossRef]
19. Wang, H.; Chai, H.; Lv, Z.; Zhang, Z.; Meng, L.; Yang, X.; Yang, T. Silicon photonic transceivers for application in data centers. *J. Semicond.* **2020**, *41*, 101301. [CrossRef]
20. Huang, A.Q. Power semiconductor devices for smart grid and renewable energy systems. In *Power Electronics in Renewable Energy Systems and Smart Grid*; Wiley: Hoboken, NJ, USA, 2019; pp. 85–152.
21. Han, B.-M.; Choi, N.-S.; Lee, J.-Y. New bidirectional intelligent semiconductor transformer for smart grid application. *IEEE Trans. Power Electron.* **2013**, *29*, 4058–4066. [CrossRef]
22. Divan, D.; Moghe, R.; Prasai, A. Power electronics at the grid edge: The key to unlocking value from the smart grid. *IEEE Power Electron. Mag.* **2014**, *1*, 16–22. [CrossRef]
23. Kaji, N.; Niwa, H.; Suda, J.; Kimoto, T. Ultrahigh-voltage SiC pin diodes with improved forward characteristics. *IEEE Trans. Electron Devices* **2014**, *62*, 374–381. [CrossRef]
24. Hower, P.L.; Pendharkar, S.; Efland, T. Current status and future trends in silicon power devices. In Proceedings of the 2010 International Electron Devices Meeting, San Francisco, CA, USA, 6–8 December 2010; pp. 13.11.11–13.11.14.
25. Iannuzzo, F.; Abbate, C.; Busatto, G. Instabilities in silicon power devices: A review of failure mechanisms in modern power devices. *IEEE Ind. Electron. Mag.* **2014**, *8*, 28–39. [CrossRef]
26. Mao, S.; Wu, T.; Lu, X.; Popovic, J.; Ferreira, J.A. High frequency high voltage power conversion with silicon carbide power semiconductor devices. In Proceedings of the 2016 6th Electronic System-Integration Technology Conference (ESTC), Grenoble, France, 13–15 September 2016; pp. 1–5.

27. Baliga, B.J. Power semiconductor device figure of merit for high-frequency applications. *IEEE Electron Device Lett.* **1989**, *10*, 455–457. [CrossRef]
28. Uhlir, A. The potential of semiconductor diodes in high-frequency communications. *Proc. IRE* **1958**, *46*, 1099–1115. [CrossRef]
29. Tournier, D.; Brosselard, P.; Raynaud, C.; Lazar, M.; Morel, H.; Planson, D. Wide band gap semiconductors benefits for high power, high voltage and high temperature applications. *Adv. Mater. Res.* **2011**, *324*, 46–51. [CrossRef]
30. Schaller, R.R. Moore's law: Past, present and future. *IEEE Spectr.* **1997**, *34*, 52–59. [CrossRef]
31. Theis, T.N.; Wong, H.-S.P. The end of moore's law: A new beginning for information technology. *Comput. Sci. Eng.* **2017**, *19*, 41–50. [CrossRef]
32. Chow, T.P.; Omura, I.; Higashiwaki, M.; Kawarada, H.; Pala, V. Smart power devices and ICs using GaAs and wide and extreme bandgap semiconductors. *IEEE Trans. Electron Devices* **2017**, *64*, 856–873. [CrossRef]
33. Shenai, K.; Scott, R.S.; Baliga, B.J. Optimum semiconductors for high-power electronics. *IEEE Trans. Electron Devices* **1989**, *36*, 1811–1823. [CrossRef]
34. Baliga, B.J. *Wide Bandgap Semiconductor Power Devices: Materials, Physics, Design, and Applications*; Woodhead Publishing: Sawston, UK, 2018.
35. Clees, T. *AMG Strategies for PDE Systems with Applications in Industrial Semiconductor Simulation*; Shaker: Herzogenrath, Germany, 2005.
36. Tan, H.; Mathews, J.A. Cyclical industrial dynamics: The case of the global semiconductor industry. *Technol. Forecast. Soc. Change* **2010**, *77*, 344–353. [CrossRef]
37. Katoh, Y.; Snead, L.L.; Henager, C., Jr.; Nozawa, T.; Hinoki, T.; Iveković, A.; Novak, S.; De Vicente, S.G. Current status and recent research achievements in SiC/SiC composites. *J. Nucl. Mater.* **2014**, *455*, 387–397. [CrossRef]
38. Jones, E.A.; Wang, F.F.; Costinett, D. Review of commercial GaN power devices and GaN-based converter design challenges. *IEEE J. Emerg. Sel. Top. Power Electron.* **2016**, *4*, 707–719. [CrossRef]
39. Islam, N.; Mohamed, M.F.P.; Khan, M.F.A.J.; Falina, S.; Kawarada, H.; Syamsul, M. Reliability, Applications and Challenges of GaN HEMT Technology for Modern Power Devices: A Review. *Crystals* **2022**, *12*, 1581. [CrossRef]
40. Quist, T.M.; Rediker, R.H.; Keyes, R.; Krag, W.; Lax, B.; McWhorter, A.L.; Zeigler, H. Semiconductor maser of GaAs. *Appl. Phys. Lett.* **1962**, *1*, 91–92. [CrossRef]
41. Ye, P.; Wilk, G.; Yang, B.; Kwo, J.; Chu, S.; Nakahara, S.; Gossmann, H.-J.; Mannaerts, J.; Hong, M.; Ng, K. GaAs metal–oxide–semiconductor field-effect transistor with nanometer-thin dielectric grown by atomic Layer deposition. *Appl. Phys. Lett.* **2003**, *83*, 180–182. [CrossRef]
42. Chang, C.; Kai, F. *GaAs High-Speed Devices: Physics, Technology, and Circuit Applications*; John Wiley & Sons: Hoboken, NJ, USA, 1994.
43. Ozkendir, O.M. Electronic structure study of Sn-substituted InP semiconductor. *Adv. J. Sci. Eng.* **2020**, *1*, 7–11.
44. Micic, O.I.; Curtis, C.J.; Jones, K.M.; Sprague, J.R.; Nozik, A.J. Synthesis and characterization of InP quantum dots. *J. Phys. Chem.* **1994**, *98*, 4966–4969. [CrossRef]
45. Hu, J.; Stoffels, S.; Zhao, M.; Tallarico, A.N.; Rossetto, I.; Meneghini, M.; Kang, X.; Bakeroot, B.; Marcon, D.; Kaczer, B. Time-dependent breakdown mechanisms and reliability improvement in edge terminated AlGaN/GaN Schottky diodes under HTRB tests. *IEEE Electron Device Lett.* **2017**, *38*, 371–374. [CrossRef]
46. Pearton, S.; Ren, F.; Zhang, A.; Lee, K. Fabrication and performance of GaN electronic devices. *Mater. Sci. Eng.* **2000**, *30*, 55–212. [CrossRef]
47. Bi, W.W.; Kuo, H.H.; Ku, P.; Shen, B. *Handbook of GaN Semiconductor Materials and Devices*; CRC Press: Boca Raton, FL, USA, 2017.
48. Pearton, S.J.; Ren, F. GaN electronics. *Adv. Mater.* **2000**, *12*, 1571–1580. [CrossRef]
49. Ayalew, T. SiC Semiconductor Devices Technology, Modeling and Simulation. Ph.D. Thesis, Technische Universität Wien, Vienna, Austria, 2004.
50. Mishra, U.K.; Parikh, P.; Wu, Y.-F. AlGaN/GaN HEMTs-an overview of device operation and applications. *Proc. IEEE* **2002**, *90*, 1022–1031. [CrossRef]
51. Kemerley, R.T.; Wallace, H.B.; Yoder, M.N. Impact of wide bandgap microwave devices on DoD systems. *Proc. IEEE* **2002**, *90*, 1059–1064. [CrossRef]
52. Das, P. High-κ Oxide Charge Engineering on GaN for Normally Off HEMTs. *J. Electron. Mater.* **2024**, *53*, 3415–3425. [CrossRef]
53. Baliga, B.J. *Fundamentals of Power Semiconductor Devices*; Springer Science & Business Media: Berlin/Heidelberg, Germany, 2010.
54. Baliga, B.J. Silicon carbide power devices: A 35 year journey from conception to commercialization. In Proceedings of the 2018 76th Device Research Conference (DRC), Santa Barbara, CA, USA, 24–27 June 2018; pp. 1–2.
55. Han, L.; Tang, X.; Wang, Z.; Gong, W.; Zhai, R.; Jia, Z.; Zhang, W. Research Progress and Development Prospects of Enhanced GaN HEMTs. *Crystals* **2023**, *13*, 911. [CrossRef]
56. Feltin, E.; Beaumont, B.; Laügt, M.; De Mierry, P.; Vennéguès, P.; Lahreche, H.; Leroux, M.; Gibart, P. Stress control in GaN grown on silicon (111) by metalorganic vapor phase epitaxy. *Appl. Phys. Lett.* **2001**, *79*, 3230–3232. [CrossRef]
57. Khan, M.A.; Van Hove, J.; Kuznia, J.; Olson, D. High electron mobility GaN/$Al_xGa_{1-x}N$ heterostructures grown by low-pressure metalorganic chemical vapor deposition. *Appl. Phys. Lett.* **1991**, *58*, 2408–2410. [CrossRef]
58. del Alamo, J.A.; Joh, J. GaN HEMT reliability. *Microelectron. Reliab.* **2009**, *49*, 1200–1206. [CrossRef]
59. Joshin, K.; Kikkawa, T.; Masuda, S.; Watanabe, K. Outlook for GaN HEMT technology. *Fujitsu Sci. Tech. J.* **2014**, *50*, 138–143.

60. Asbeck, P.M. Electronic properties of III-nitride materials and basics of III-nitride FETs. In *III-Nitride Electronic Devices*; Semiconductors and Semimetals; Elsevier Ltd.: Amsterdam, The Netherlands, 2019; pp. 1–40.
61. Okita, H.; Kaifu, K.; Mita, J.; Yamada, T.; Sano, Y.; Ishikawa, H.; Egawa, T.; Jimbo, T. High transconductance AlGaN/GaN-HEMT with recessed gate on sapphire substrate. *Phys. Status Solidi (A)* **2003**, *200*, 187–190. [CrossRef]
62. Burnham, S.D.; Boutros, K.; Hashimoto, P.; Butler, C.; Wong, D.W.; Hu, M.; Micovic, M. Gate-recessed normally-off GaN-on-Si HEMT using a new O_2-BCl_3 digital etching technique. *Phys. Status Solidi C* **2010**, *7*, 2010–2012. [CrossRef]
63. Asubar, J.T.; Kawabata, S.; Tokuda, H.; Yamamoto, A.; Kuzuhara, M. Enhancement-mode AlGaN/GaN MIS-HEMTs with high V_{TH} and high I_{Dmax} using recessed-structure with regrown AlGaN barrier. *IEEE Electron Device Lett.* **2020**, *41*, 693–696. [CrossRef]
64. Uemoto, Y.; Hikita, M.; Ueno, H.; Matsuo, H.; Ishida, H.; Yanagihara, M.; Ueda, T.; Tanaka, T.; Ueda, D. Gate injection transistor (GIT)—A normally-off AlGaN/GaN power transistor using conductivity modulation. *IEEE Trans. Electron Devices* **2007**, *54*, 3393–3399. [CrossRef]
65. Greco, G.; Iucolano, F.; Roccaforte, F. Review of technology for normally-off HEMTs with p-GaN gate. *Mater. Sci. Semicond. Process.* **2018**, *78*, 96–106. [CrossRef]
66. Brannick, A.; Zakhleniuk, N.A.; Ridley, B.K.; Shealy, J.R.; Schaff, W.J.; Eastman, L.F. Influence of field plate on the transient operation of the AlGaN/GaN HEMT. *IEEE Electron Device Lett.* **2009**, *30*, 436–438. [CrossRef]
67. Dora, Y.; Chakraborty, A.; Mccarthy, L.; Keller, S.; DenBaars, S.; Mishra, U. High breakdown voltage achieved on AlGaN/GaN HEMTs with integrated slant field plates. *IEEE Electron Device Lett.* **2006**, *27*, 713–715. [CrossRef]
68. Fletcher, A.A.; Nirmal, D.; Ajayan, J.; Arivazhagan, L. Analysis of AlGaN/GaN HEMT using discrete field plate technique for high power and high frequency applications. *AEU-Int. J. Electron. Commun.* **2019**, *99*, 325–330. [CrossRef]
69. Hasan, M.T.; Asano, T.; Tokuda, H.; Kuzuhara, M. Current collapse suppression by gate field-plate in AlGaN/GaN HEMTs. *IEEE Electron Device Lett.* **2013**, *34*, 1379–1381. [CrossRef]
70. Srour, J.R.; Marshall, C.J.; Marshall, P.W. Review of displacement damage effects in silicon devices. *IEEE Trans. Nucl. Sci.* **2003**, *50*, 653–670. [CrossRef]
71. Malik, A.; Sharma, C.; Laishram, R.; Bag, R.K.; Rawal, D.S.; Vinayak, S.; Sharma, R.K. Role of AlGaN/GaN interface traps on negative threshold voltage shift in AlGaN/GaN HEMT. *Solid-State Electron.* **2018**, *142*, 8–13. [CrossRef]
72. Zhang, W.; Zhang, Y.; Mao, W.; Ma, X.; Zhang, J.; Hao, Y. Influence of the interface acceptor-like traps on the transient response of AlGaN/GaN HEMTs. *IEEE Electron Device Lett.* **2012**, *34*, 45–47. [CrossRef]
73. Hao, R.; Fu, K.; Yu, G.; Li, W.; Yuan, J.; Song, L.; Zhang, Z.; Sun, S.; Li, X.; Cai, Y.; et al. Normally-off p-GaN/AlGaN/GaN high electron mobility transistors using hydrogen Plasma treatment. *Appl. Phys. Lett.* **2016**, *109*, 152106. [CrossRef]
74. Yong, C.; Yugang, Z.; Chen, K.J.; Lau, K.M. High-performance enhancement-mode AlGaN/GaN HEMTs using fluoride-based Plasma treatment. *IEEE Electron Device Lett.* **2005**, *26*, 435–437. [CrossRef]
75. Shul, R.; McClellan, G.; Casalnuovo, S.; Rieger, D.; Pearton, S.; Constantine, C.; Barratt, C.; Karlicek, R.; Tran, C.; Schurman, M. Inductively coupled Plasma etching of GaN. *Appl. Phys. Lett.* **1996**, *69*, 1119–1121. [CrossRef]
76. Pearton, S.; Shul, R.; Ren, F. A review of dry etching of GaN and related materials. *Mater. Res. Soc. Internet J. Nitride Semicond. Res.* **2000**, *5*, e11. [CrossRef]
77. Cheung, R.; Rong, B.; van der Drift, E.; Sloof, W. Etch mechanism and etch-induced effects in the inductively coupled Plasma etching of GaN. *J. Vac. Sci. Technol. B* **2003**, *21*, 1268–1272. [CrossRef]
78. Smith, S.; Wolden, C.; Bremser, M.; Hanser, A.; Davis, R.; Lampert, W. High rate and selective etching of GaN, AlGaN, and AlN using an inductively coupled Plasma. *Appl. Phys. Lett.* **1997**, *71*, 3631–3633. [CrossRef]
79. Nakamura, S. The roles of structural imperfections in InGaN-based blue light-emitting diodes and laser diodes. *Science* **1998**, *281*, 956–961. [CrossRef] [PubMed]
80. Mouffak, Z.; Bensaoula, A.; Trombetta, L. The effects of nitrogen Plasma on reactive-ion etching induced damage in GaN. *J. Appl. Phys.* **2004**, *95*, 727–730. [CrossRef]
81. King, S.; Barnak, J.; Bremser, M.; Tracy, K.; Ronning, C.; Davis, R.; Nemanich, R. Cleaning of AlN and GaN surfaces. *J. Appl. Phys.* **1998**, *84*, 5248–5260. [CrossRef]
82. Belkind, A.; Gershman, S. Plasma cleaning of surfaces. In *Surface Contamination*; Springer: Boston, MA, USA, 2008; pp. 46–57. [CrossRef]
83. Petasch, W.; Kegel, B.; Schmid, H.; Lendenmann, K.; Keller, H. Low-pressure Plasma cleaning: A process for precision cleaning applications. *Surf. Coat. Technol.* **1997**, *97*, 176–181. [CrossRef]
84. Choi, H.; Chua, S.; Tripathy, S. Morphological and structural analyses of Plasma-induced damage to n-type GaN. *J. Appl. Phys.* **2002**, *92*, 4381–4385. [CrossRef]
85. Wang, X.; Yu, G.; Lei, B.; Wang, X.; Lin, C.; Sui, Y.; Meng, S.; Qi, M.; Li, A. Recovery of dry etching–induced damage in n-GaN by nitrogen Plasma treatment at growth temperature. *J. Electron. Mater.* **2007**, *36*, 697–701. [CrossRef]
86. Lee, J.-M.; Chang, K.-M.; Kim, S.-W.; Huh, C.; Lee, I.-H.; Park, S.-J. Dry etch damage in n-type GaN and its recovery by treatment with an N 2 Plasma. *J. Appl. Phys.* **2000**, *87*, 7667–7670. [CrossRef]
87. Cao, X.-A.; Pearton, S.J.; Ren, F. Advanced processing of GaN for electronic devices. *Crit. Rev. Solid State Mater. Sci.* **2000**, *25*, 279–390. [CrossRef]
88. Wang, R.; Cai, Y.; Chen, K.J. Temperature dependence and thermal stability of planar-integrated enhancement/depletion-mode AlGan/GaN HEMTs and digital circuits. *Solid-State Electron.* **2009**, *53*, 1–6. [CrossRef]

89. Hao, R.; Xu, N.; Yu, G.; Song, L.; Chen, F.; Zhao, J.; Deng, X.; Li, X.; Cheng, K.; Fu, K.; et al. Studies on Fabrication and Reliability of GaN High-Resistivity-Cap-Layer HEMT. *IEEE Trans. Electron Devices* **2018**, *65*, 1314–1320. [CrossRef]
90. Nakamura, S.; Iwasa, N.; Senoh, M.S.M.; Mukai, T.M.T. Hole compensation mechanism of p-type GaN films. *Jpn. J. Appl. Phys.* **1992**, *31*, 1258. [CrossRef]
91. Polyakov, A.; Smirnov, N.; Govorkov, A.; Baik, K.; Pearton, S.; Luo, B.; Ren, F.; Zavada, J. Hydrogen Plasma passivation effects on properties of p-GaN. *J. Appl. Phys.* **2003**, *94*, 3960–3965. [CrossRef]
92. Chen, S.; Ishikawa, K.; Lu, Y.; Kometani, R.; Kondo, H.; Tokuda, Y.; Egawa, T.; Amano, H.; Sekine, M.; Hori, M. Individual Roles of Atoms and Ions during Hydrogen Plasma Passivation of Surface Defects on GaN Created by Plasma Etching. *Jpn. J. Appl. Phys.* **2012**, *51*, 111002. [CrossRef]
93. Hu, X.; Simin, G.; Yang, J.; Khan, M.A.; Gaska, R.; Shur, M. Enhancement mode AlGaN/GaN HFET with selectively grown pn junction gate. *Electron. Lett.* **2000**, *36*, 753–754. [CrossRef]
94. Chang, T.-F.; Hsiao, T.-C.; Huang, C.-F.; Kuo, W.-H.; Lin, S.-F.; Samudra, G.S.; Liang, Y.C. Phenomenon of drain current instability on p-GaN gate AlGaN/GaN HEMTs. *IEEE Trans. Electron Devices* **2014**, *62*, 339–345. [CrossRef]
95. Han, Y.; Xue, S.; Guo, W.; Luo, Y.; Hao, Z.; Sun, C. Highly selective dry etching of GaN over AlGaN using inductively coupled Cl2/N2/O2 Plasmas. *Jpn. J. Appl. Phys.* **2003**, *42*, L1139. [CrossRef]
96. Li, F.; Liang, Y.; Zhang, Y.; Huang, Y.; Li, A.; Zhu, Y.; Yu, C.; Wang, Y.; Wu, S.; Yu, G.; et al. Monolithic Investigation of Hydrogen Plasma-Treated and Etched p-GaN Gate HEMTs Under OFF-State Drain Stress. *IEEE Trans. Electron Devices* **2024**, *71*, 3801–3804. [CrossRef]
97. Wei, J.; Xie, R.; Xu, H.; Wang, H.; Wang, Y.; Hua, M.; Zhong, K.; Tang, G.; He, J.; Zhang, M. Charge Storage Mechanism of Drain Induced Dynamic Threshold Voltage Shift in p-GaN Gate HEMTs. *IEEE Electron Device Lett.* **2019**, *40*, 526–529. [CrossRef]
98. Chen, J.; Hua, M.; Wei, J.; He, J.; Wang, C.; Zheng, Z.; Chen, K.J. OFF-state drain-voltage-stress-induced V TH instability in Schottky-type p-GaN gate HEMTs. *IEEE J. Emerg. Sel. Top. Power Electron.* **2020**, *9*, 3686–3694. [CrossRef]
99. Efthymiou, L.; Murukesan, K.; Longobardi, G.; Udrea, F.; Shibib, A.; Terrill, K. Understanding the threshold voltage instability during OFF-state stress in p-GaN HEMTs. *IEEE Electron Device Lett.* **2019**, *40*, 1253–1256. [CrossRef]
100. Johnson, N.; Burnham, R.; Street, R.; Thornton, R. Hydrogen passivation of shallow-acceptor impurities in p-type GaAs. *Phys. Rev. B* **1986**, *33*, 1102. [CrossRef] [PubMed]
101. Sun, C.; Ding, X.; Wei, X.; Tang, W.; Zhang, X.; Zhao, D.; Li, S.; Yu, G.; Song, L.; Cai, Y.; et al. Reduced Reverse Gate Leakage Current for p-GaN Gate High-Electron-Mobility Transistors by a Surface-Etching Method. *Phys. Status Solidi (A)* **2021**, *218*, 2000666. [CrossRef]
102. Qian, Q.; Zhang, Z.; Hua, M.; Tang, G.; Lei, J.; Lan, F.; Xu, Y.; Yan, R.; Chen, K.J. Enhanced dielectric deposition on single-Layer MoS_2 with low damage using remote N_2 Plasma treatment. *Nanotechnology* **2017**, *28*, 175202. [CrossRef] [PubMed]
103. Wang, Y.; Gui, D.; Kumar, R.; Foo, P. Reduction of oxygen Plasma damage by postdeposition helium Plasma treatment for carbon-doped silicon oxide low dielectric constant films. *Electrochem. Solid-State Lett.* **2002**, *6*, F1. [CrossRef]
104. Huang, X.; Xing, Y.; Yu, G.; Tang, W.; Wei, X.; Song, L.; Zhang, X.; Fan, Y.; Zeng, Z.; Cai, Y.; et al. The effect of SiN_x film for H Plasma implantation in p-GaN/AlGaN/GaN high electron mobility transistors. *Appl. Phys. Express* **2022**, *15*, 071010. [CrossRef]
105. Huang, X.-J.; Xing, Y.-H.; Yu, G.-H.; Song, L.; Huang, R.; Huang, Z.-L.; Han, J.; Zhang, B.-S.; Fan, Y.-M. Study on H Plasma treatment enhanced p-GaN gate AlGaN/GaN HEMT with block Layer. *Acta Phys. Sin.* **2022**, *71*, 108501. [CrossRef]
106. Xing, Y.; Han, Z.; Huang, X.; Yu, G.; Yin, C.; Guan, B.; Han, J.; Zhang, B.; Zeng, Z. The effect of Si_3N_4/Al_2O_3 stacked structure of AlGaN/GaN HEMTs. *Microelectron. Reliab.* **2023**, *151*, 115263. [CrossRef]
107. Hao, R.; Wu, D.; Fu, K.; Song, L.; Chen, F.; Zhao, J.; Du, Z.; Zhang, B.; Wang, Q.; Yu, G.; et al. 10 A/567 V normally off p-GaN gate HEMT with high-threshold voltage and low-gate leakage current. *Electron. Lett.* **2018**, *54*, 848–849. [CrossRef]
108. Hao, R.; Sun, C.; Fang, B.; Xu, N.; Tao, Z.; Zhang, H.; Wei, X.; Lin, W.; Zhang, X.; Yu, G.; et al. Monolithic integration of enhancement/depletion-mode high electron mobility transistors using hydrogen Plasma treatment. *Appl. Phys. Express* **2019**, *12*, 036502. [CrossRef]
109. Wei, X.; Zhang, X.; Sun, C.; Tang, W.; Zeng, C.; Chen, F.; He, T.; Yu, G.; Song, L.; Lin, W.; et al. Improvement of Breakdown Voltage and ON-Resistance in Normally-OFF AlGaN/GaN HEMTs Using Etching-Free p-GaN Stripe Array Gate. *IEEE Trans. Electron Devices* **2021**, *68*, 5041–5047. [CrossRef]
110. Nomoto, K.; Chaudhuri, R.; Bader, S.J.; Li, L.; Hickman, A.; Huang, S.; Lee, H.; Maeda, T.; Then, H.W.; Radosavljevic, M. GaN/AlN p-Channel HFETs with I_{max} > 420 mA/mm and ~20 GHz f_T/f_{MAX}. In Proceedings of the 2020 IEEE International Electron Devices Meeting (IEDM), San Francisco, CA, USA, 12–18 December 2020; pp. 8.3.1–8.3.4.
111. Chowdhury, N.; Lemettinen, J.; Xie, Q.; Zhang, Y.; Rajput, N.S.; Xiang, P.; Cheng, K.; Suihkonen, S.; Then, H.W.; Palacios, T. P-Channel GaN transistor based on p-GaN/AlGaN/GaN on Si. *IEEE Electron Device Lett.* **2019**, *40*, 1036–1039. [CrossRef]
112. Wei, J.; Tang, G.; Xie, R.; Chen, K.J. GaN power IC technology on p-GaN gate HEMT platform. *Jpn. J. Appl. Phys.* **2020**, *59*, SG0801. [CrossRef]
113. Zheng, Z.; Song, W.; Zhang, L.; Yang, S.; Xu, H.; Wong, R.K.-Y.; Wei, J.; Chen, K.J. Enhancement-mode GaN p-Channel MOSFETs for power integration. In Proceedings of the 2020 32nd International Symposium on Power Semiconductor Devices and ICs (ISPSD), Vienna, Austria, 13–18 September 2020; pp. 525–528.
114. Zheng, Z.; Song, W.; Zhang, L.; Yang, S.; Wei, J.; Chen, K.J. High I_{ON} and I_{ON}/I_{OFF} Ratio Enhancement-Mode Buried p-Channel GaN MOSFETs on p-GaN Gate Power HEMT Platform. *IEEE Electron Device Lett.* **2019**, *41*, 26–29. [CrossRef]

115. Zheng, Z.; Zhang, L.; Song, W.; Chen, T.; Feng, S.; Ng, Y.H.; Sun, J.; Xu, H.; Yang, S.; Wei, J. Threshold voltage instability of enhancement-mode GaN buried p-Channel MOSFETs. *IEEE Electron Device Lett.* **2021**, *42*, 1584–1587. [CrossRef]
116. Yang, C.; Fu, H.; Peri, P.; Fu, K.; Yang, T.-H.; Zhou, J.; Montes, J.; Smith, D.J.; Zhao, Y. Enhancement-Mode Gate-Recess-Free GaN-Based p-Channel Heterojunction Field-Effect Transistor With Ultra-Low Subthreshold Swing. *IEEE Electron Device Lett.* **2021**, *42*, 1128–1131. [CrossRef]
117. Gao, X.; Yu, G.; Zhou, J.; Wang, Z.; Li, Y.; Zhang, J.; Liang, X.; Zeng, Z.; Zhang, B. Study of enhancement-mode GaN pFET with H Plasma treated gate recess. *J. Semicond.* **2023**, *44*, 112801. [CrossRef]
118. Tang, W.-X.; Hao, R.-H.; Chen, F.; Yu, G.-H.; Zhang, B.-S. P-GaN hybrid anode AlGaN/GaN diode with 1000 V operation. *Acta Phys. Sin.* **2018**, *67*, 198501. [CrossRef]
119. Cao, X.; Zhang, A.; Dang, G.; Cho, H.; Ren, F.; Pearton, S.; Shul, R.; Zhang, L.; Hickman, R.; Van Hove, J. Inductively coupled Plasma damage in GaN Schottky diodes. *J. Vac. Sci. Technol. B* **1999**, *17*, 1540–1544. [CrossRef]
120. Wei, X.; Zhang, X.; Zhou, X.; Ma, Y.; Tang, W.; Chen, T.; Liu, W.; Tang, W.; Yu, G.; Fan, Y.; et al. Dual Current and Voltage Sensitivity Temperature Sensor Based on Lateral p-GaN/AlGaN/GaN Hybrid Anode Diode. *IEEE Sens. J.* **2021**, *21*, 22459–22463. [CrossRef]
121. Yang, A.; Wei, X.; Shen, W.; Hu, Y.; Chen, T.; Wang, H.; Zhou, J.; Xing, R.; Zhang, X.; Yu, G.; et al. Highly Reliable Temperature Sensor Based on p-GaN/AlGaN/GaN Hybrid Anode Diode with Wide Operation Temperature from 73 K to 573 K. *Crystals* **2023**, *13*, 620. [CrossRef]
122. Fu, H.; Fu, K.; Liu, H.; Alugubelli, S.R.; Huang, X.; Chen, H.; Montes, J.; Yang, T.-H.; Yang, C.; Zhou, J.; et al. Implantation-and etching-free high voltage vertical GaN p–n diodes terminated by Plasma-hydrogenated p-GaN: Revealing the role of thermal annealing. *Appl. Phys. Express* **2019**, *12*, 051015. [CrossRef]
123. Fu, K.; He, Z.; Yang, C.; Zhou, J.; Fu, H.; Zhao, Y. GaN-on-GaN p-i-n diodes with avalanche capability enabled by eliminating surface leakage with hydrogen Plasma treatment. *Appl. Phys. Lett.* **2022**, *121*, 092103. [CrossRef]
124. Fu, H.; Fu, K.; Alugubelli, S.R.; Cheng, C.-Y.; Huang, X.; Chen, H.; Yang, T.-H.; Yang, C.; Zhou, J.; Montes, J.; et al. High Voltage Vertical GaN p-n Diodes With Hydrogen-Plasma Based Guard Rings. *IEEE Electron Device Lett.* **2020**, *41*, 127–130. [CrossRef]
125. Rongming, C.; Chang Soo, S.; Man Hoi, W.; Fichtenbaum, N.; Brown, D.; McCarthy, L.; Keller, S.; Feng, W.; Speck, J.S.; Mishra, U.K. Impact of CF_4 Plasma Treatment on GaN. *IEEE Electron Device Lett.* **2007**, *28*, 781–783. [CrossRef]
126. Kawakami, R.; Nakano, Y.; Niibe, M.; Shirahama, T.; Mukai, T. Electrical Investigation of Deep-Level Defects Introduced in AlGaN/GaN Heterostructures by CF_4 Plasma Treatments. *ECS Solid State Lett.* **2015**, *4*, P36–P38. [CrossRef]
127. Ma, Y.; Chen, C.; Hong, Y.; Cai, Y. Two-photon process in F treated AlGaN/GaN heterojunction HEMT device. In Proceedings of the 2022 19th China International Forum on Solid State Lighting & 2022 8th International Forum on Wide Bandgap Semiconductors (SSLCHINA: IFWS), Suzhou, China, 7–10 February 2023; pp. 55–57.
128. Nakano, Y.; Kawakami, R.; Niibe, M. Generation of electrical damage in n-GaN films following treatment in a CF4Plasma. *Appl. Phys. Express* **2017**, *10*, 116201. [CrossRef]
129. Cai, Y.; Cheng, Z.; Tang, W.C.W.; Lau, K.M.; Chen, K.J. Monolithically Integrated Enhancement/Depletion-Mode AlGaN/GaN HEMT Inverters and Ring Oscillators Using CF_4 Plasma Treatment. *IEEE Trans. Electron Devices* **2006**, *53*, 2223–2230. [CrossRef]
130. Wang, R.; Cai, Y.; Tang, C.W.; Lau, K.M.; Chen, K.J. Enhancement-Mode Si_3N_4/AlGaN/GaN MISHFETs. *IEEE Electron Device Lett.* **2006**, *27*, 793–795. [CrossRef]
131. Dong, Z.; Tan, S.; Cai, Y.; Chen, H.; Liu, S.; Xu, J.; Xue, L.; Yu, G.; Wang, Y.; Zhao, D.; et al. 5.3A/400V normally-off AlGaN/GaN-on-Si MOS-HEMT with high threshold voltage and large gate swing. *Electron. Lett.* **2013**, *49*, 221–222. [CrossRef]
132. Ding, X.; Song, L.; Yu, G.; Cai, Y.; Sun, Y.; Zhang, B.; Du, Z.; Zeng, Z.; Zhang, X.; Zhang, B. Gate leakage mechanisms of the AlGaN/GaN HEMT with fluorinated graphene passivation. *Mater. Sci. Semicond. Process.* **2023**, *162*, 107502. [CrossRef]
133. Palacios, T.; Suh, C.S.; Chakraborty, A.; Keller, S.; DenBaars, S.P.; Mishra, U.K. High-performance E-mode AlGaN/GaN HEMTs. *IEEE Electron Device Lett.* **2006**, *27*, 428–430. [CrossRef]
134. Liu, C.; Yang, S.; Liu, S.; Tang, Z.; Wang, H.; Jiang, Q.; Chen, K.J. Thermally Stable Enhancement-Mode GaN Metal-Isolator-Semiconductor High-Electron-Mobility Transistor With Partially Recessed Fluorine-Implanted Barrier. *IEEE Electron Device Lett.* **2015**, *36*, 318–320. [CrossRef]
135. Park, Y.; Kim, J.; Chang, W.; Jung, D.; Bae, S.; Mun, J.; Jun, C.H.; Ko, S.; Nam, E. Normally-off GaN MIS-HEMT using a combination of recessed-gate structure and CF_4 Plasma treatment. *Phys. Status Solidi (A)* **2015**, *212*, 1170–1173. [CrossRef]
136. Yang, L.; Hou, B.; Mi, M.; Zhu, Q.; Wu, M.; Zhu, J.; Lu, Y.; Zhang, M.; Chen, L.; Zhou, X.; et al. High-Performance Enhancement-mode AlGaN/GaN high electron mobility transistors combined with TiN-based Source Contact Ledge and Two-Step Fluorine Treatment. *IEEE Electron Device Lett.* **2018**, *39*, 1544–1547. [CrossRef]
137. Ma, Y.; Chen, L.; Dong, Z.; Hong, Y.; Xiao, Y.; Xin, Y.; Zhang, B.; Qin, H.; Zhang, T.; Zhang, X.; et al. Current Drops in CF_4 Plasma-Treated AlGaN/GaN Heterojunction in Polar Gas Ambient. *Electronics* **2023**, *12*, 1809. [CrossRef]
138. Ridley, B.; Ambacher, O.; Eastman, L.F. The polarization-induced electron gas in a heterostructure. *Semicond. Sci. Technol.* **2000**, *15*, 270. [CrossRef]
139. Ibbetson, J.P.; Fini, P.; Ness, K.; DenBaars, S.; Speck, J.; Mishra, U. Polarization effects, surface states, and the source of electrons in AlGaN/GaN heterostructure field effect transistors. *Appl. Phys. Lett.* **2000**, *77*, 250–252. [CrossRef]

140. Song, D.; Liu, J.; Cheng, Z.; Tang, W.C.W.; Lau, K.M.; Chen, K.J. Normally Off AlGaN/GaN Low-Density Drain HEMT (LDD-HEMT) With Enhanced Breakdown Voltage and Reduced Current Collapse. *IEEE Electron Device Lett.* **2007**, *28*, 189–191. [CrossRef]
141. Fornasiero, Q.; Defrance, N.; Lepilliet, S.; Avramovic, V.; Cordier, Y.; Frayssinet, E.; Lesecq, M.; Idir, N.; De Jaeger, J.-C. Fabrication, and Direct Current and cryogenic analysis of SF_6-treated AlGaN/GaN Schottky barrier diodes. *J. Vac. Sci. Technol. B* **2023**, *41*, 012202. [CrossRef]
142. Liu, K.; Wang, C.; Zheng, X.; Ma, X.; Zhao, Y.; Li, A.; He, Y.; Mao, W.; Hao, Y. Improving the Performance of Deep Recessed Anode AlGaN/GaN Schottky Barrier Diode by Post Etching Treatment. *Phys. Status Solidi (A)* **2021**, *218*, 2000686. [CrossRef]
143. Linkohr, S.; Pletschen, W.; Polyakov, V.; Himmerlich, M.; Lorenz, P.; Krischok, S.; Kirste, L.; Müller, S.; Ambacher, O.; Cimalla, V. Influence of Plasma treatments on the properties of GaN/AlGaN/GaN HEMT structures. *Phys. Status Solidi C* **2012**, *9*, 1096–1098. [CrossRef]
144. Hashizume, T.; Nakasaki, R. Discrete surface state related to nitrogen-vacancy defect on Plasma-treated GaN surfaces. *Appl. Phys. Lett.* **2002**, *80*, 4564–4566. [CrossRef]
145. Kucheyev, S.O.; Williams, J.S.; Pearton, S.J. Ion implantation into GaN. *Mater. Sci. Eng.* **2001**, *33*, 51–108. [CrossRef]
146. Zkria, A.; Katamune, Y.; Yoshitake, T.; Ohmagari, S.; Hanada, T. P-type doping of GaN by magnesium ion implantation. *Appl. Phys. Express* **2017**, *10*, 016501.
147. Wang, M.; Yuan, L.; Chen, K.; Xu, F.; Shen, B. Diffusion mechanism and the thermal stability of fluorine ions in GaN after ion implantation. *J. Appl. Phys.* **2009**, *105*, 083519. [CrossRef]
148. Wang, M.; Chen, K.J. Improvement of the Off-State Breakdown Voltage With Fluorine Ion Implantation in AlGaN/GaN HEMTs. *IEEE Trans. Electron Devices* **2011**, *58*, 460–465. [CrossRef]
149. Chen, H.; Wang, M.; Chen, K.J. Enhancement-Mode AlGaN/GaN HEMTs Fabricated by Standard Fluorine Ion Implantation with a Si_3N_4 Energy-Absorbing Layer. *Electrochem. Solid-State Lett.* **2011**, *14*, H229–H231. [CrossRef]
150. Zhang, Z.; Fu, K.; Deng, X.; Zhang, X.; Fan, Y.; Sun, S.; Song, L.; Xing, Z.; Huang, W.; Yu, G.; et al. Normally Off AlGaN/GaN MIS-High-Electron Mobility Transistors Fabricated by Using Low Pressure Chemical Vapor Deposition Si_3N_4 Gate Dielectric and Standard Fluorine Ion Implantation. *IEEE Electron Device Lett.* **2015**, *36*, 1128–1131. [CrossRef]
151. Sun, J.; Zhang, Z.; Li, X.; Qin, H.; Sun, Y.; Cai, Y.; Yu, G.; Zhang, Z.; Zhang, J.; Shangguan, Y.; et al. Two-terminal terahertz detectors based on AlGaN/GaN high-electron-mobility transistors. *Appl. Phys. Lett.* **2019**, *115*, 111101. [CrossRef]
152. Parikh, N.; Suvkhanov, A.; Lioubtchenko, M.; Carlson, E.; Bremser, M.; Bray, D.; Davis, R.; Hunn, J. Ion implantation of epitaxial GaN films: Damage, doping and activation. *Nucl. Instrum. Methods Phys. Res. Sect. B* **1997**, *127*, 463–466. [CrossRef]
153. Posselt, M.; Schmidt, B.; Murthy, C.; Feudel, T.; Suzuki, K. Modeling of Damage Accumulation during Ion Implantation into Single-Crystalline Silicon. *J. Electrochem. Soc.* **1997**, *144*, 1495. [CrossRef]
154. Heft, A.; Wendler, E.; Heindl, J.; Bachmann, T.; Glaser, E.; Strunk, H.; Wesch, W. Damage production and annealing of ion implanted silicon carbide. *Nucl. Instrum. Methods Phys. Res. Sect. B* **1996**, *113*, 239–243. [CrossRef]
155. Shen, F.; Hao, R.; Song, L.; Chen, F.; Yu, G.; Zhang, X.; Fan, Y.; Lin, F.; Cai, Y.; Zhang, B. Enhancement mode AlGaN/GaN HEMTs by fluorine ion thermal diffusion with high Vth stability. *Appl. Phys. Express* **2019**, *12*, 066501. [CrossRef]
156. Yang, S.; Tang, Z.; Wong, K.-Y.; Lin, Y.-S.; Liu, C.; Lu, Y.; Huang, S.; Chen, K.J. High-Quality Interface in Al_2O_3/GaN/GaN/AlGaN/GaN MIS Structures With In Situ Pre-Gate Plasma Nitridation. *IEEE Electron Device Lett.* **2013**, *34*, 1497–1499. [CrossRef]
157. Zhang, Z.; Li, W.; Fu, K.; Yu, G.; Zhang, X.; Zhao, Y.; Sun, S.; Song, L.; Deng, X.; Xing, Z.; et al. AlGaN/GaN MIS-HEMTs of Very-Low Vth Hysteresis and Current Collapse With In-Situ Pre-Deposition Plasma Nitridation and LPCVD-Si_3N_4 Gate Insulator. *IEEE Electron Device Lett.* **2017**, *38*, 236–239. [CrossRef]
158. Lu, S.; Yu, G.; Sun, Y.; Yuan, X.; Du, Z.; Zhang, B.; Wang, L.; Li, Y.; Wu, D.; Huang, Z.; et al. p-GaN Selective Nitridation to Obtain a Normally Off p-GaN Gate AlGaN/GaN High-Electron-Mobility Transistors. *Phys. Status Solidi (RRL)-Rapid Res. Lett.* **2023**, *18*, 2300301. [CrossRef]
159. Akasaki, I.; Amano, H. Widegap column-III nitride semiconductors for UV/blue light emitting devices. *J. Electrochem. Soc.* **1994**, *141*, 2266. [CrossRef]
160. Kaufmann, U.; Kunzer, M.; Maier, M.; Obloh, H.; Ramakrishnan, A.; Santic, B.; Schlotter, P. Nature of the 2.8 eV photoluminescence band in Mg doped GaN. *Appl. Phys. Lett.* **1998**, *72*, 1326–1328. [CrossRef]
161. Sun, C.; Hao, R.; Xu, N.; He, T.; Shi, F.; Yu, G.; Song, L.; Huang, Z.; Huang, R.; Zhao, Y.; et al. Normally-off p-GaN/AlGaN/GaN high-electron-mobility transistors using oxygen Plasma treatment. *Appl. Phys. Express* **2019**, *12*, 051001. [CrossRef]
162. Xu, S.; Zhou, Y.; Zhang, X.; Li, Q.; Liu, J.; Qie, H.; Wang, Q.; Zhan, X.; Sun, X.; Dai, Q.; et al. Effects of ammonia and oxygen Plasma treatment on interface traps in AlGaN/GaN metal–insulator–semiconductor high-electron-mobility transistors. *Appl. Phys. Lett.* **2023**, *123*, 203504. [CrossRef]
163. Pankove, J.; Torvik, J.; Qiu, C.-H.; Grzegory, I.; Porowski, S.; Quigley, P.; Martin, B. Molecular doping of gallium nitride. *Appl. Phys. Lett.* **1999**, *74*, 416–418. [CrossRef]
164. Baliga, B.J. Gallium nitride devices for power electronic applications. *Semicond. Sci. Technol.* **2013**, *28*, 074011. [CrossRef]
165. Wu, C.-H.; Han, P.-C.; Luc, Q.H.; Hsu, C.-Y.; Hsieh, T.-E.; Wang, H.-C.; Lin, Y.-K.; Chang, P.-C.; Lin, Y.-C.; Chang, E.Y. Normally-OFF GaN MIS-HEMT With F− Doped Gate Insulator Using Standard Ion Implantation. *IEEE J. Electron Devices Soc.* **2018**, *6*, 893–899. [CrossRef]

166. Yang, S.; Huang, S.; Schnee, M.; Zhao, Q.-T.; Schubert, J.; Chen, K.J. Enhancement-mode LaLuO3–AlGaN/GaN metal–insulator–semiconductor high-electron-mobility transistors using fluorine Plasma ion implantation. *Jpn. J. Appl. Phys.* **2013**, *52*, 08JN02. [CrossRef]
167. Tang, Z.; Jiang, Q.; Lu, Y.; Huang, S.; Yang, S.; Tang, X.; Chen, K.J. 600-V normally off SiN_x/AlGaN/GaN MIS-HEMT with large gate swing and low current collapse. *IEEE Electron Device Lett.* **2013**, *34*, 1373–1375. [CrossRef]

Disclaimer/Publisher's Note: The statements, opinions and data contained in all publications are solely those of the individual author(s) and contributor(s) and not of MDPI and/or the editor(s). MDPI and/or the editor(s) disclaim responsibility for any injury to people or property resulting from any ideas, methods, instructions or products referred to in the content.